Fermi National Accelerator Laboratory

FN-364
1502.000

# PRODUCTION OF ELECTRONS AND POSITRONS BY IMPINGING 100 GeV PROTONS ON A TARGET FOR PURPOSE OF FILLING AN ELECTRON STORAGE RING

S. Conetti
Institute for Particle Physics, Montreal, Canada

and

A. G. Ruggiero
Fermi National Accelerator Laboratory, Batavia, Illinois 60510

April 1982

Operated by Universities Research Association Inc. under contract with the United States Department of Energy

## I. Introduction

To avoid seriously limiting coherent instability and too much beam loading on the RF system, it is convenient to inject in an electron storage ring at as high an energy as possible, preferably at the same energy that the storage ring is supposed to operate when in the colliding-mode. This, though, would be very expensive and requires larger and more complex accelerators operating as injectors.

As an alternative we propose here an interesting idea (see V.I. Balbekov et al. , Xth International Conference on High Energy Accelerators, Protvino, USSR, July 1977, Vol. I, p. 177) to produce pairs of electrons and positrons by impinging primary protons on a target. This idea works very well and it is mostly suited for the Fermilab electron-proton proposals. Indeed Fermilab has already available a large energy and intense proton beam as a source.

The scheme we propose is similar to the one to collect antiprotons (The Fermilab Antiproton Source Design Report, February 1982). The major differences are that it is much easier to collect electrons and positrons, the yield from a target being two orders of magnitude larger, and that with electrons there is automatically a "cooling" technique to collect them. This is done by the synchrotron radiation damping, a cooling system which is reliable, extremely fast and inexpensive.

The scheme is simple and it can be understood by inspecting Figure 1 which shows the Fermilab site with all the accelerators and storage rings that will exist at one time or another. Figure 2 gives a closer look at the region around D0 where Main Ring, Tevatron and the electron storage ring touch each other.

The proton beam is accelerated as usual to 100 GeV. At this energy there is a small flat-top to allow for some rf manipulations that will be described in the following section. When the beam is ready it is extracted in several pulses, each with about the length of the electron storage ring. The extraction occurs at C17. The proton beam is taken to a target where $e^{\pm}$-pairs are produced. A transport line takes the chosen charge ($e^+$ or $e^-$) down to the electron storage ring where the beam is injected and stored. After a period of three betatron damping times the beam has been "cooled" and now the next proton beam segment can be extracted from the Main Ring to produce more $e^{\pm}$-pairs. This is repeated until the Main Ring is empty, at which time the cycle repeats.

In section III we discuss the targeting of the proton beam and the capture of the $e^{\pm}$'s in the storage ring. In section IV we show in detail our yield calculations.

We took under consideration two cases. One is a 5 GeV storage ring proposed by Columbia University and the other is a 10 GeV storage ring (CHEER) proposed by a Canadian group. The relevant parameters for these two rings are summarized in Table I.

We make the assumption that the bunching of the electron beam in the storage ring and the bunching of the proton beam in the Tevatron are the same and that corresponds, for both cases, to one bunch every 7 RF buckets in the Tevatron at 53 MHz. It is convenient to prepare the proton beam before targeting to produce $e^{\pm}$-beam already at the required bunching. Moreover, the bunching of one bunch every 7 RF buckets, corresponds to a beam gap of 130 nsec that can be used for the fall-off time of an extraction kicker in the Tevatron or a rise-time of an injection magnet in the electron storage ring.

We found filling times for the required intensities that ranges between a few minutes to several tens of minutes. This is short enough to make the idea quite attractive especially for the positron beam production.

## II. Main Ring RF Manipulation and Preparation of the Proton Beam for Targeting

The Main Ring cycle is shown in Figure 3. The Main Ring is filled-up as usual, in the box-car fashion at 8.0 GeV, with 13 Booster batches, for a total of $3\times10^{13}$ protons. The beam is bunched with the standard 53.1 MHz, h=1113, RF system.

Before acceleration, three consecutive bunches every seven are eliminated with the fast, transverse super-damper as shown in Figure 4. This is a conventional technique at Fermilab.

The beam is then accelerated to 100 GeV where the cycle has a flat-top 0.3 sec. long.

We assume that each bunch, with careful adjustment of injection and transition energy crossing, has a longitudinal phase space area of 0.2 eV-sec and $3\times10^{10}$ particles. The beam is made of a total of $1.7\times10^{13}$ protons.

During flat-top the beam will undergo two major RF manipulations similar to those that have already been proposed for the Fermilab $\bar{p}$ source.

### Phase I

At the end of the acceleration the beam is kept bunched by stationary buckets produced by the 4 MV, 53 MHz RF system. As first step the RF voltage will be turned off slowly so that the beam will adiabatically debunch. It takes about 10 msec to do this, which corresponds to two phase oscillations at 4 MV/turn.

It is not possible to turn the RF off completely to zero, because of multipactoring problems and beam loading. The minimum voltage that can be reached is probably 10 kV, so the beam will not be completely debunched but will extend over ±180° as shown in Figure 5. Bunches will touch each other.

At this stage it is proper to approximate four consecutive bunches as a single one with rectangular shape. The longitudinal phase space area of this larger bunch is

$$S = \frac{\pi}{2} \times 4 \times 0.2 \simeq 1.3 \text{ eV-sec}$$

Each superbunch has $1.2\times10^{11}$ protons, the length

$$\sigma_\tau = \pm 38 \text{ nsec}$$

and the height

$$\Delta E = \pm 8.6 \text{ MeV}$$

At this point the voltage of a 7.586 MHz RF system is turned on as quickly as one can, say within one turn, that is 20 $\mu$sec. This RF system corresponds to the harmonic number $h=1113\div 7 = 159$ and creates stationary buckets to capture the superbunches as shown at the bottom of Figure 5.

Since the shape of the superbunches is mismatched to the trajectories of the h=159 stationary buckets, the superbunches will rotate as shown in Figure 6.

We require that after a quarter of the phase oscillation the beam has a maximum energy spread

$$\frac{\Delta E}{E} = \pm 0.1\%$$

that is $\Delta E = \pm 101$ MeV, and a bunch length

$$\sigma_\tau = \pm 3.2 \text{ nsec}$$

The required bucket height is

$$\Delta E_b = \sqrt{2}\, \Delta E = \pm 143 \text{ MeV}$$

which corresponds to the RF voltage

$$V = 140 \text{ kV}$$

at 7.586 MHz.

The bunch rotation takes a quarter of phase oscillation, that is about 20 msec.

As soon as the bunch rotation is accomplished one switches immediately to the 53 MHz RF system again. The 7.6 MHz is turned off at the same time the 53 MHz RF system is turned on, that is within one period (20 $\mu$sec).

We require the voltage is set so that the shape of the bunch is matched to the new 53 MHz stationary bucket to stop the rotation of the bunches. For this purpose the bucket height

$$\Delta E_b = \frac{\Delta E}{\sin \phi/2}$$

where $\Delta E = \pm 101$ MeV is the beam height and

$\phi = \pm 180° \times 3.2$ nsec/9.4 nsec $= \pm 61°$ the bunch extension:

$$\Delta E_b = 200 \text{ MeV}$$

This corresponds to a voltage V = 1.9 MV at 53 MHz. At the end of this phase one has about 150 superbunches occupying one out of seven of the 53 MHz RF stationary buckets. Bunches are separated by about 130 nsec, have a longitudinal phase space area of 1.3 eV-sec and $1.2 \times 10^{11}$ protons each.

The RF manipulation we have described above has also been proposed to combine 4 Main Ring bunches in one single superbunch for proton-antiproton collision in the Tevatron. Computer simulations to check the scheme exist

(K. Takayama, J. MacLachlan) and a preliminary experiment has already been tried successfully (J. Griffin and J. MacLachlan).

Phase II

For targeting it is important to make the proton bunches as narrow as possible so that also the $e^{\pm}$-bunches are narrow enough to match the RF buckets in the electron storage ring.

The following RF manipulation has also been proposed for targeting protons to produce antiprotons (Fermilab, 1982 Antiproton Source Design).

The 53 MHz voltage is turned down slowly until bunches extend over ±90°. The voltage is turned down in 13 msec, which corresponds to two phase oscillations with 1.9 MV/turn. In the following we shall assume the bunches have elliptical shape. At the end of the adiabatic voltage drop:

$$V = 750 \text{ kV}$$

$$\Delta E = \pm 88 \text{ MeV}$$

$$\sigma_\tau = \pm 4.7 \text{ nsec}$$

The bunch shape is continuously matched to the trajectories of the RF bucket.

Suddenly the voltage is turned on to full value (4 MV) within one turn ($\sim$20 μsec). We want to point out that RF voltage modulation at this proposed rate has already been demonstrated experimentally for the Main Ring. The bunch is now mismatched and will rotate in the similar fashion as illustrated in Figure 6.

At 4 MV/turn the bucket height is

$$E_b = \pm 290 \text{ MeV}$$

and the beam height after a quarter of phase oscillation (which lasts 1.3 msec) is

$$E = \pm 205 \text{ MeV}$$

which corresponds to a new length

$$\sigma_\tau = \pm 2.0 \text{ nsec}$$

The result depends on the individual bunch area before any RF manipulation is applied, here assumed to be 0.2 eV-sec. The final bunch length could be a factor of two smaller (±1.0 nsec) if the bunch area were also a factor of two smaller at the start (0.1 eV-sec).

Right after a quarter of the phase oscillation has been completed and the beam bunchees are the narrowest, a segment of the beam is extracted, targeted to produce the same number of $e^{\pm}$-bunches spaced by 130 nsec and injected in the electron storage ring in one single turn.

The bunches remaining in the Main Ring will continue to rotate for another quarter of phase oscillation, until they extend again over a phase of ±90°. At this time the RF voltage is dropped again, and very fast, to 750 kV.

As we have seen at this level, the bunches are matched and stop rotating. The beam in the Main Ring is kept under these conditions as long as necessary, until the e-bunches in the electron storage ring have been "cooled" enough in all directions by the synchrotron radiation. Typically this takes three betatron damping times, that is a total period of time that can range from 10 to 50 msec depending on the energy and the size of the electron storage ring.

When a new segment is ready for extraction and targeting the bunch rotation of phase II is repeated again. This will go on until the Main Ring is empty.

The length of the flat-top in the MR cycle is calculated as the sum of the duration of the steps we have described above:

$$t_{\text{flat-top}} = 10 \text{ msec} + 20 \text{ msec} + 15 \text{ msec} + (n-1)(3\tau_{\text{damping}})$$

where n is the number of pulses injected in the electron storage ring per Main Ring cycle. For the two rings shown in Table I we have at most $t_{\text{flat-top}} = 0.23$ sec. Therefore a Main Ring cycle of 3.0 seconds sounds more than reasonable.

Finally observe that although extraction from the Main Ring at 100 GeV with a beam gap of 130 nsec appears to be possible, we did not investigate the requirements it would impose upon the whole extraction system.

## III. Proton Target and Electron Capture

At 100 GeV the proton emittance is $\varepsilon_H = \varepsilon_V = 0.223\pi\ 10^{-6}$ m, which include, 95% of the beam with bi-gaussian distribution.

The proton beam can be focused on a target where $\beta_H^* = \beta_V^* = 1$ m so that the rms beam spot size is

$$\sigma_H = \sigma_V = 0.193 \text{ mm}$$

To avoid onset of shock waves that could result in the density depletion of the target the energy-density deposition should be of no more than 200 J/g. With the beams cross section specified above the maximum number of protons that one can impinge on the target at one time is

$$N_p = 7.8\times10^{11}$$

for a target 5 cm long (see the Fermilab Antiproton Source Design Report).

The target we are actually considering here for $e^{\pm}$-pair production will be several times longer (40 cm) and therefore we should be capable to impinge on the target a number of protons in excess of $10^{12}$. As we can see from Table I, the actual number of protons hitting the target during one pulse does not exceed $10^{12}$, so that our choice of $\beta_H^* = \beta_V^* = 1$ m is reasonable.

As a collector we can use a lithium lens similar to the one proposed for the antiproton collection. With this lens one can focus on a plane in the target where $\beta_H^* = \beta_V^* = 10$ cm for the electrons.

The maximum number of electrons (positrons) that can be captured depends eventually on the momentum aperture and betatron acceptance of the storage ring, that we estimate here to be about

$$\frac{\Delta p}{p} = \pm 1\%$$

$$A_H = A_V = 20\pi\ 10^{-6}\ \mathrm{m}$$

With a $\beta^*$=10 cm this corresponds to a beam size of ±1.5 mm and an angle of ±15 mrad at the focal plane, assuming there zero dispersion.

Each electron bunch accepted will have therefore a momentum spread of ±1% with a roughly uniform distribution and a longitudinal gaussian distribution of the same width as proton bunches. As we have seen in the previous section the width for 95% of the beam is ±2 nsec.

Nevetheless only those electrons that will fall in the moving buckets created by the RF cavities in the storage ring will be captured. The bucket height and length are given in Table I. It turns out that the Columbia storage ring can capture considerably more electrons because, due to the RF choice, the buckets are longer and wider.

We estimate that only about 20% of the electrons will be RF captured for CHEER but as much 50% will be captured in the Columbia storage ring.

After three damping times of the betatron oscillations the injected beam is "cooled" to the equilibrium values which are shown also in Table I. These values are considerably smaller than those at the injection and there is plenty of room for injection of subsequent pulses.

## IV. Yield Calculations

We have prepared a Monte Carlo computer simulation to estimate the yield of electron and positron pairs produced by protons on a target. The chain of reaction we have considered is the following:

$$
\begin{aligned}
p + Be &\rightarrow \pi^{0} + X \\
&\quad \hookrightarrow \gamma\gamma \\
&\qquad\quad \hookrightarrow e^{+}+e^{-} \\
&\qquad\quad \hookrightarrow e^{+}+e^{-}
\end{aligned}
$$

In order to maximize the acceptance of the electron transport line, we propose to use the same target both for producing the $\pi^{0}$s and to convert the photons. Given the ratio of momenta of the incoming protons and outgoing electrons (100 vs 5 or 10 GeV), it is important not to let the $e^{-}$ electromagnetic shower grow, so as not to degrade the electron's momenta. For these reasons we choose a beryllium target (absorption length $\sim$ radiation length) 40 cm long and wide enough so that particles do not escape radially. A more detailed study would be required to determine the optimum target length, but our simple minded Monte Carlo showed the value of 40 cm to be quite reasonable.

(i) The initial conditions for the proton beam are first generated. We generate a proton by assigning four coordinate variables

$$x,\ x' \text{ and } y,\ y'$$

taken randomly according to a gaussian distribution in any of the four variables with zero means and standard deviation values given by

$$\sigma_x = \sqrt{\varepsilon\beta_x^*} \qquad \sigma_y = \sqrt{\varepsilon\beta_y^*}$$

$$\sigma_{x'} = \sqrt{\varepsilon/\beta_x^*} \qquad \sigma_{y'} = \sqrt{\varepsilon/\beta_y^*}$$

with $\varepsilon=3.72\times10^{-8}$ m the rms emittance, and $\beta_x^*=\beta_y^*=1$ m the lattice values at the focus which is assumed at the center of the target. At the focus there is a waist, that is $\beta_x'=\beta_y'=0$. The initial conditions generated correspond to the location of the focus but then the actual initial coordinates at the beginning of the target (s=0) are calculated by a single transposition

$$x \rightarrow x - x'\,\ell/2$$

$$y \rightarrow y - y'\,\ell/2$$

$$x' \rightarrow x'$$

$$y' \rightarrow y'$$

and the angles, x', y' are unchanged.

The distributions of the particles so generated at the focus location are shown in Figures 7, 8, 9, and 10. Note that these, as well as the following figures represent the result of generating 10,000 protons.

The dispersion at the focus is zero and the protons have been generated all with the same momentum.

(ii) Protons are made to interact in the taget with an exponential distribution $e^{-s/\lambda}$, $\lambda$=36.7 cm (Fig. 11). Only primary interactions are taken into account, so that the final electron/positron yield will be somewhat underestimated, since we are not keeping track of $\pi^0$'s generated in secondary interactions.

A parameterization for the longitudinal and transversal momentum distributions of the production $\pi^0$'s was obtained by averaging the $\pi^+$ and $\pi^-$ production data, as measured in the bubble chamber. Such a choice was motivated by the fact that better data exists for the charged than for the neutral $\pi$'s over the kinematical region of more copious production. Again this approximation will lead to a certain underestimate of the final yield, since photons originated from $\eta$ production and decay are neglected.

The parameterization employed was obtained from the 200 GeV data of Kafha et al., Phys. Rev. D16, 1977, 1261 and one of the form ($X_F$ being the scaling variable $p^*/p^*_{max}$)

$$E\frac{d\sigma}{dX_F} \sim e^{-(B|X_F|+C|X_F|^2)} \qquad (1)$$

with B = 4.35
C = 4.50

and

$$\frac{d\sigma}{dp_\perp^2} \sim e^{-6p_\perp^2} \qquad (2)$$

Although it is known that the transverse momentum distribution is not completely independent of $X_F$, the variations over the region of interest are small enough that the use of a factorized expression gives a very reasonable approximation. Comparison with data measured at 100 and 400 GeV (C. Bromberg et al., Nucl. Phys. B, 107, 1976, 82) guaranteed the validity of scaling in the $X_F$ and p variables, making legitimate the use of the parameterization obtained at 200 GeV.

The results of R.D. Kass et al., Phys. Rev. D20, 1979, 605 were used to obtain the average $\pi^0$ multiplicity, which is measured to be equal to 3 at 100 GeV.

Operationally, for each interacting proton three $\pi^0$'s were generated: for each $\pi^0$ a value of $-1<X_F<1$ was chosen by sampling the distribution (1); next a value for p distributed according to (2) was obtained in the range $0<p<p^{***}=(s/2)\sqrt{1-X_F{}^2}$. The azimuthal angle was then thrown with a flat probability.

The distribution of the $\pi^0$'s in the four-dimensional phase space (x,x',y,y') is shown in Figures 12, 13, 14, and 15.

The momentum distributin of the $\pi^0$'s is shown in Figure 16.

(iii) The $\pi^0$ mesons are made to decay immediately in a pair of $\gamma$'s. The decay distribution is obtained by picking at random the center of mass decay angle $\theta_\pi$. Lorentz transformations yield for the lab momenta of the two gammas

$$p_1 = \frac{1}{2} m_\pi c \gamma (1+\beta_\pi \cos\theta)$$

$$p_2 = \frac{1}{2} m_\pi c \gamma (1-\beta_\pi \cos\theta)$$

and for the respective angles of production from the direction of motion of the $\pi_o$

$$\theta_1 = \arcsin \left(\frac{m_\pi c}{2p_1} \sin \theta_\pi\right)$$

$$\theta_2 = - \arcsin \left(\frac{m_\pi c}{2p_2} \sin \theta_\pi\right)$$

The azimuthal angle is also generated randomly.

The distribution of the first gamma in x',y' and momentum ($p_1$) is shown in Figures 17, 18, and 19. The data for the second gamma are shown in Figures 20, 21, and 22. The distribution in x and y, of course, are the same as the $\pi^o$'s.

(iv) The gammas so generated will travel down the target and then will convert in pairs of $e^+e^-$.

We have used conversion length of 45.4 cm. The distribution of the coordinate for the gamma conversion is given in Figure 23. The distribution of the x,x',y,y' coordinates at the moment of conversion are shown in Figures 24, 25, 26, and 27. The momenta of the electrons are obtained from a flat momentum distribution and consequently the positron momentum is derived from

$$p_{e^+} + p_{e^-} = p_\gamma$$

The opening angle of the produced pairs, being of the order of $m_e/E_e$ is neglected, so that the pair is produced with the same direction of motion of the converting gamma. The momentum of the electrons and positrons at production is given in Figures 28 and 29 respectively.

Finally, the $e^\pm$ have a chance by traveling down the remaining part of the target to loose some amount of energy by bremmstrahlung. Figures 30 and 31 show the distribution of the coordinate where radiation occurs. We have assumed a radiation length of 35.3 cm. The energy lost is chosen according to a 1/E distribution. The final momentum distribution is given in Figures 32 and 33.

(v) We assume that a collector lens is located beyond the target. The focal plane of the collector is taken to be 15 cm downstream from the beginning of the target. The distributions of the electrons and positrons in the (x,x') and (y,y') planes projected back at the focal plane are shown in Figures 34, 35, 36, and 37. The characteristic butterfly shape is easily recognized.

The diagrams given in Figures 38, 39, 40, 41 and in Figures 42, 43, 44, 45 show the phase space distribution for $e^+$ at the desired momenta of 5 and 10 GeV (±5%) respectively.

In these diagrams we have outlined an ellipse with semi-axis of 1.45 mm and 14.5 mrad which corresponds to an acceptance 20π mm-mrad in both planes.

The yield for a 20π mm-mrad acceptance in both planes and ±5% momentum bite is attained by dividing the total number of particles falling within the ellipse by 10,000, the number of protons generated in our Monte Carlo simulation. In Table I we give the yield for ±1% momentum bite. As one can see, two minutes are required to fill up a 5 GeV electron storage ring as proposed by Columbia University. On the other hand, CHEER, the 10 GeV Canadian proposed ring would take about an hour. Nevertheless the betatron acceptance in CHEER is much larger than considered here and is capable of capturing more electrons, provided the RF frequency is lowered from 804 MHz to 496 MHz. In this case, the filling time could be less than ten minutes.

Table I. Comparison Between Two Different Energy Cases

| | CHEER | Columbia |
|---|---|---|
| Energy, GeV | 10 | 5 |
| Radius, m | 283.0 | 56.6 |
| RF Frequency, MHz | 804 | 496 |
| RF Peak Voltage, MV | 24.8 | 6.0 |
| Energy Loss, MeV/turn | 9.66 | 3.51 |
| Momentum Compaction Factor, $\alpha$ | 0.00583 | 0.00250 |
| No. of Bunches | 45 | 9 (21) |
| No. of Electr./Bunch | $10^{11}$ | $0.58\times10^{11}$ |
| Bucket Height, $\Delta p/p$ | ±0.51% | ±1.15% |
| Bucket Length, nsec | 0.73 | 0.97 |
| Harmonic No. | 4770 | 588 |
| $\sin\phi_s$ | 0.390 | 0.585 |
| Betatron Damping Time, msec | 12.2 | 3.7 |
| rms Bunch Length, nsec | 0.03 | 0.05 |
| rms Bunch Energy Spread | 0.085% | 0.1% |
| rms Betatron Emittance with Full Coupling, $10^{-6}$ m | 0.025 | 0.065 |
| No. of Proton Pulses per MR Cycle | 4 | 18 |
| MR Flat Top Length, msec | 145 | 225 |
| No. of protons per pulse on the target | $7.7\times10^{11}$ | $1.53\times10^{11}$ |
| Fraction of electrons captured within an acceptance of $20\pi$ mm-mrad and $\Delta E/E=\pm1\%$ | 0.2 | 0.5 |
| Yield: $N_e/N_p$ | $2.3\times10^{-4}$ | $9.2\times10^{-4}$ |
| Filling Time with a MR Cycle of 3 sec. | 3,450 sec | 100 sec |

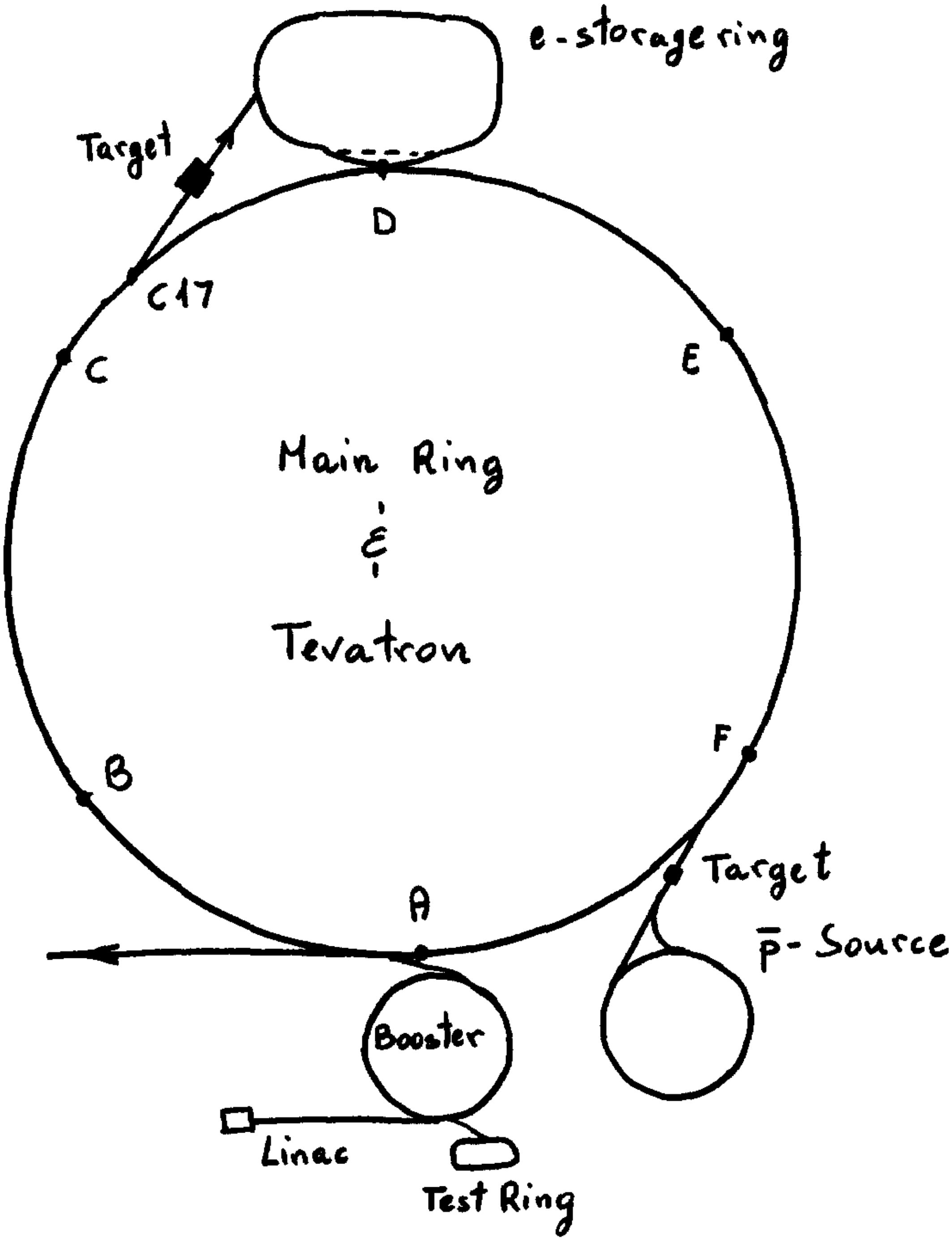


Fig. 1. Plan View of Fermilab Site

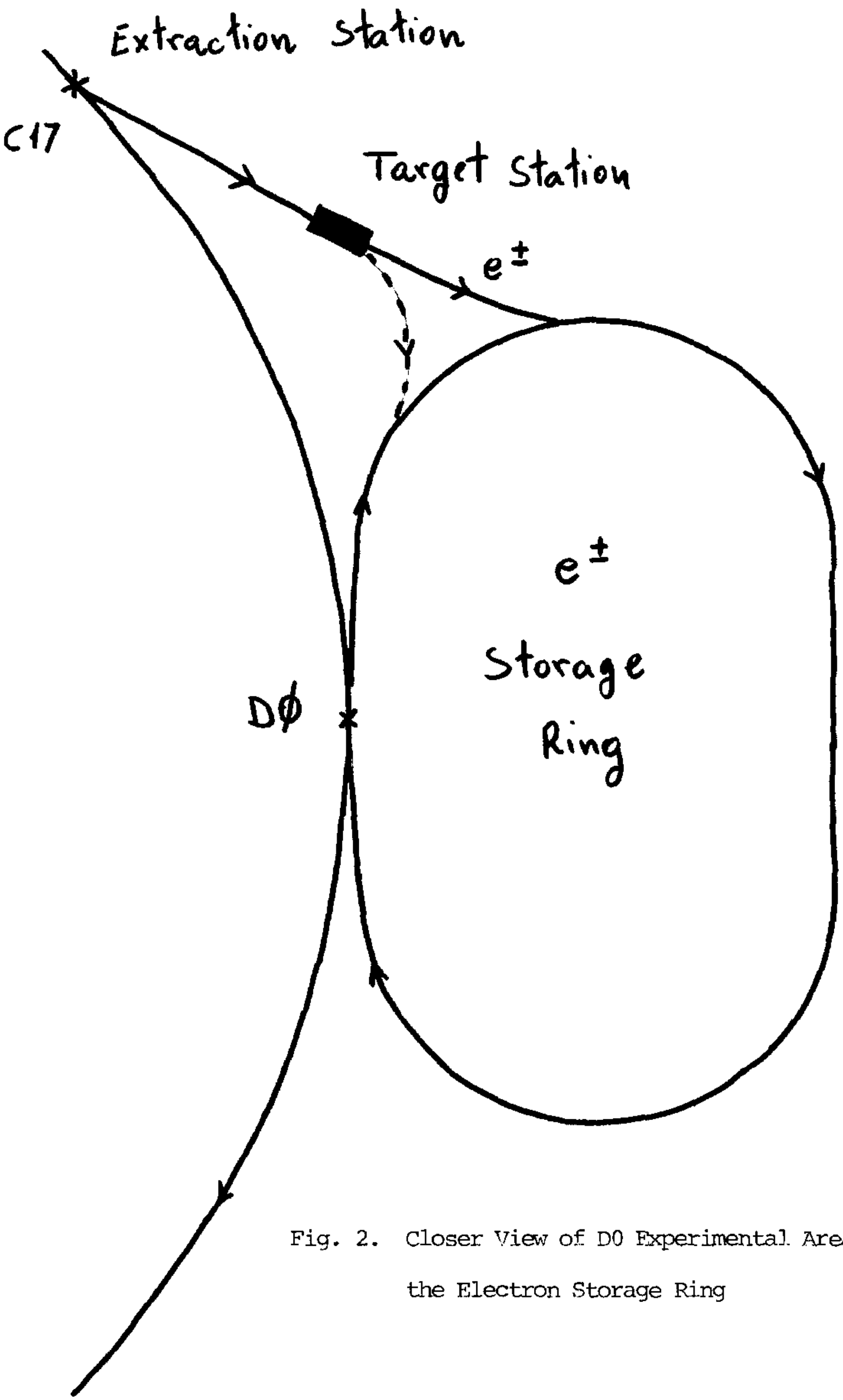


Fig. 2. Closer View of D0 Experimental Area with the Electron Storage Ring

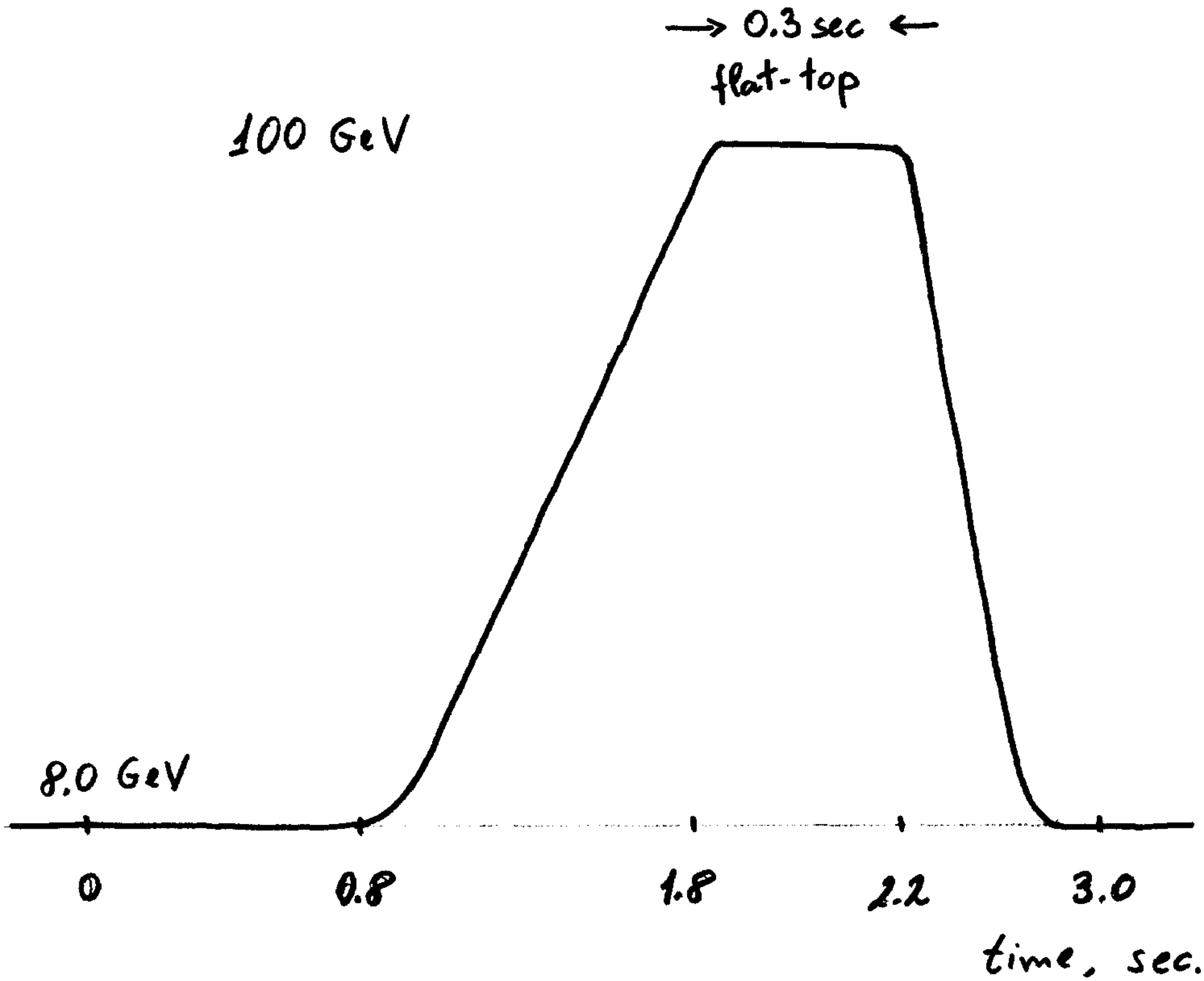


Fig. 3. Diagram of the Main Ring Cycle

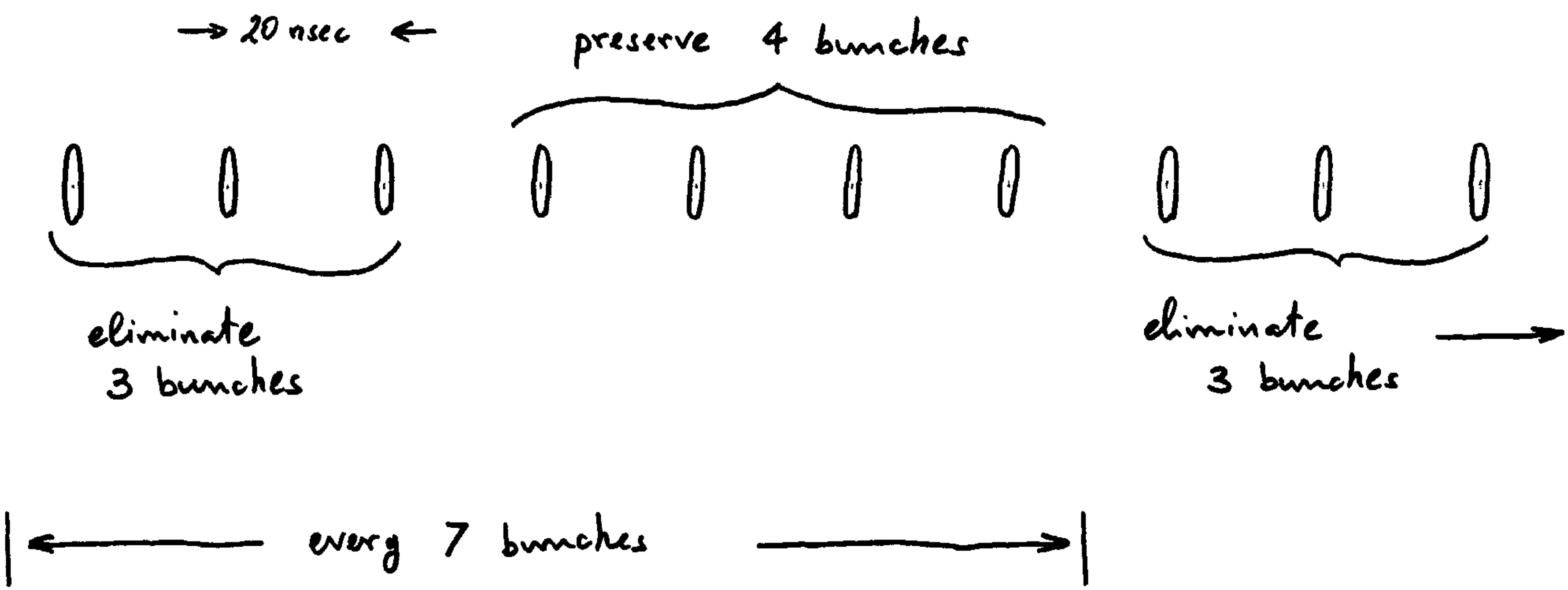


Fig. 4. Proton Beam Bunching in the Main Ring at 8.0 GeV

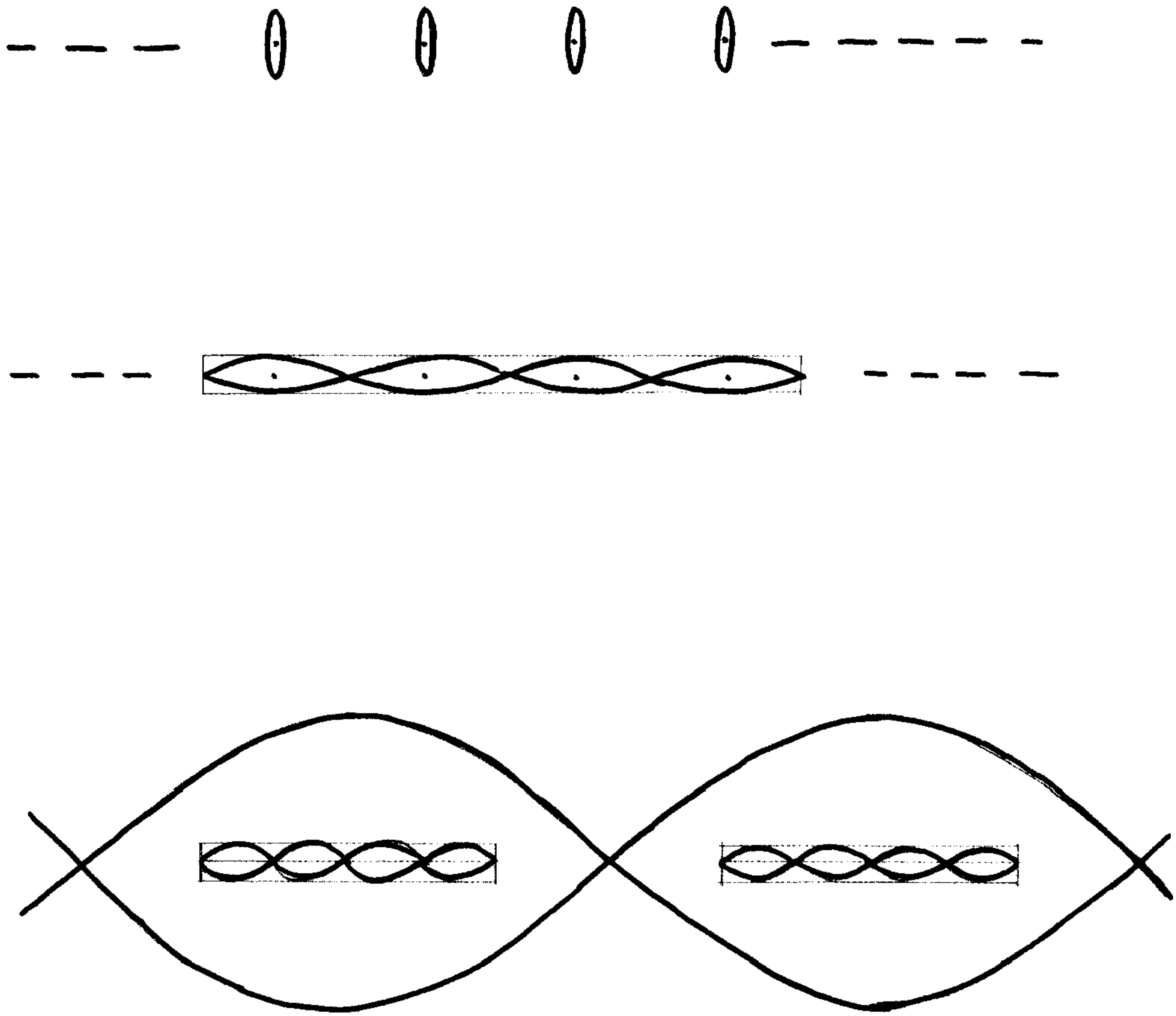

Fig. 5. Creation of the Proton Superbunches in the Main Ring

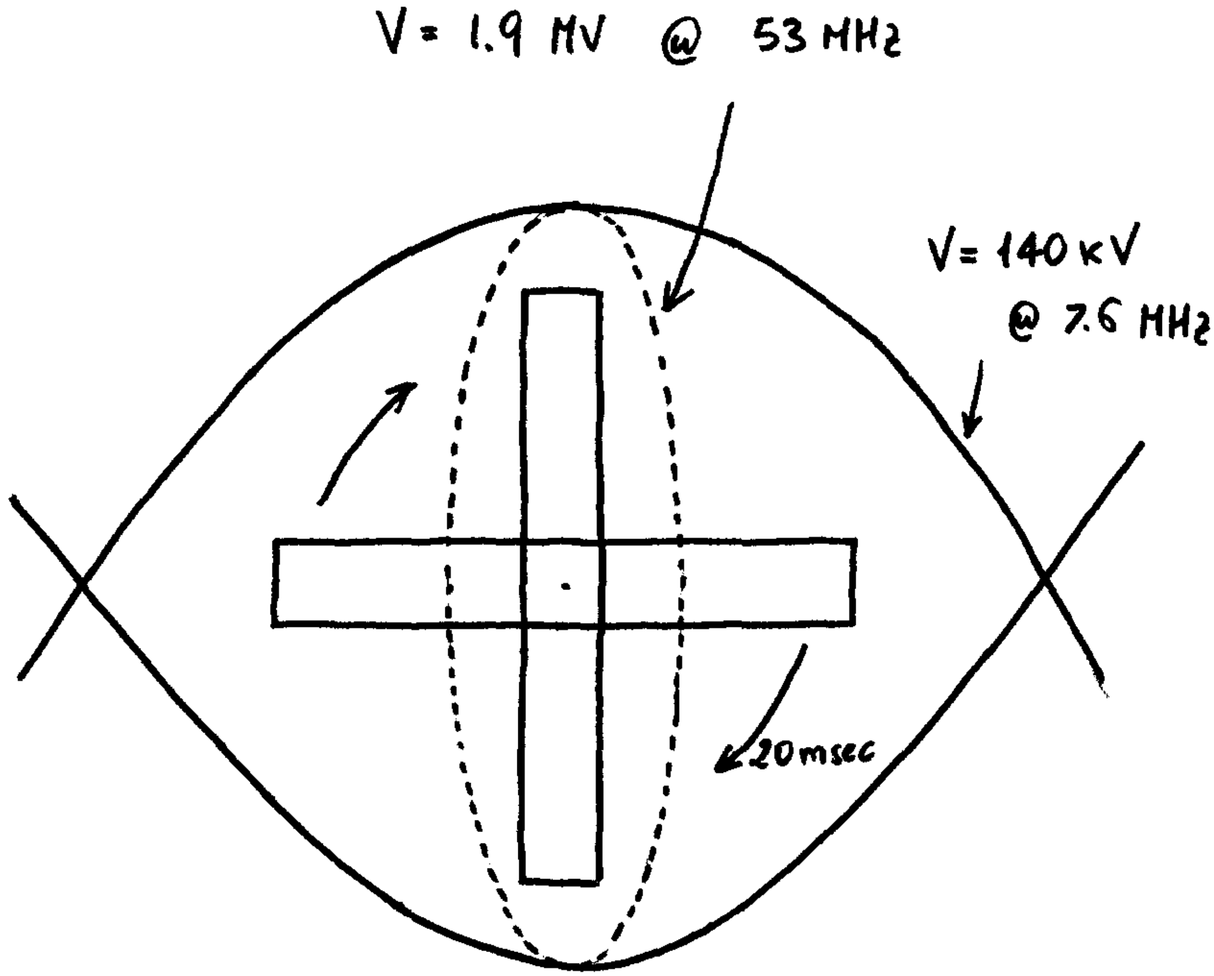


Fig. 6. Bunch Rotation at h = 159 in the Main Ring

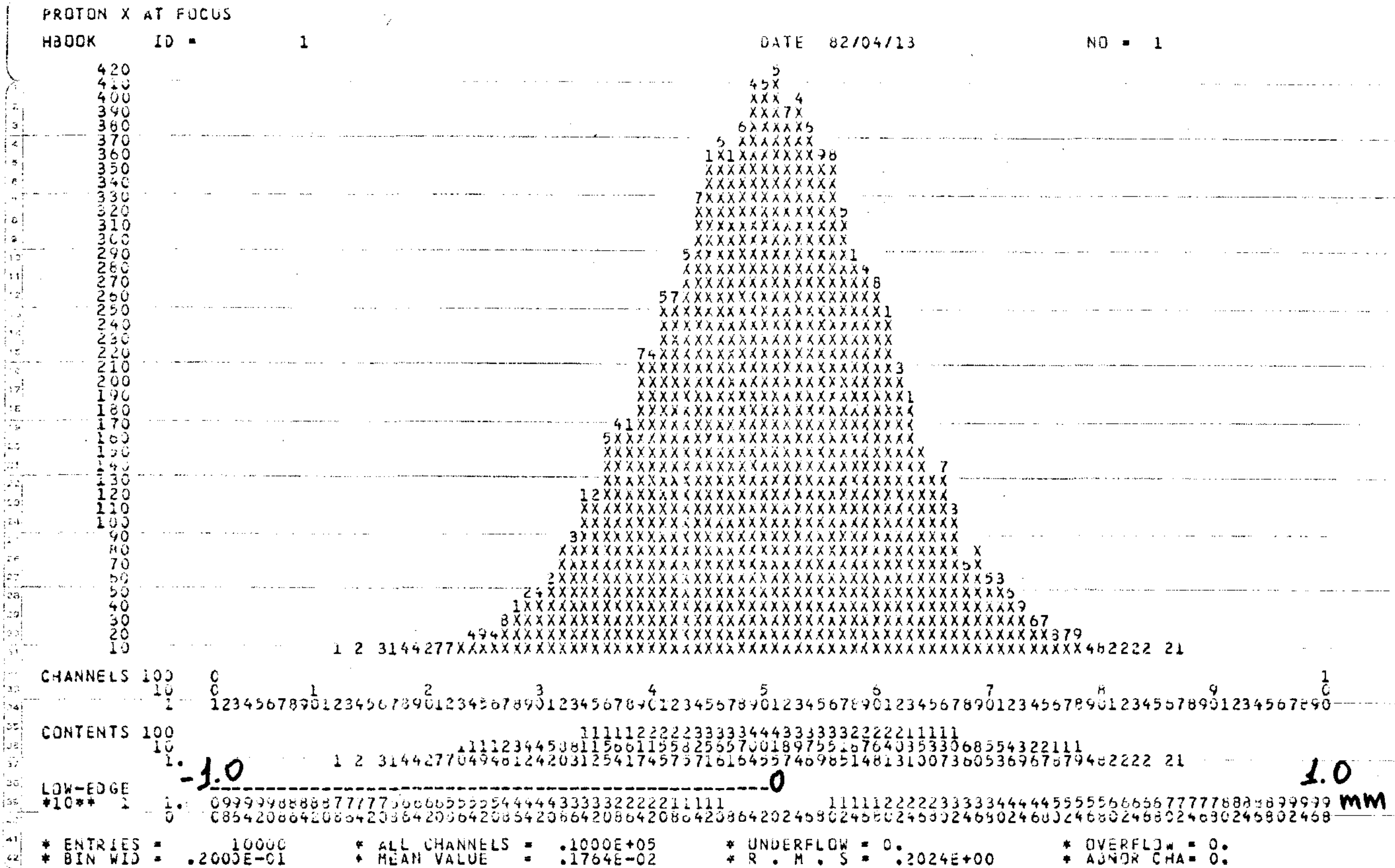


Fig. 7. Proton x - Distribution in the center of the Target ( Focus )

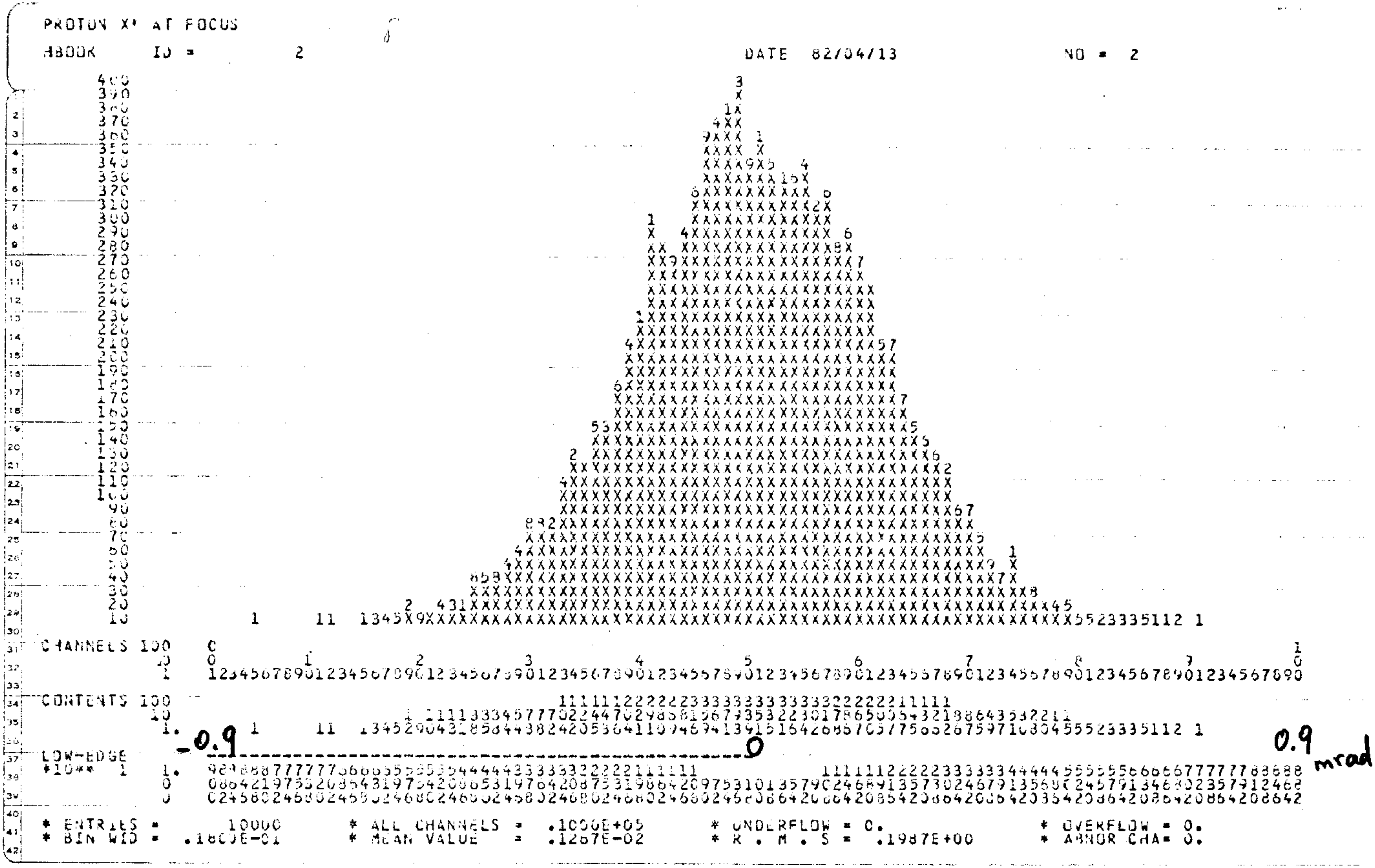


Fig. 8. Proton x' - Distribution in the center of the Target ( Focus )

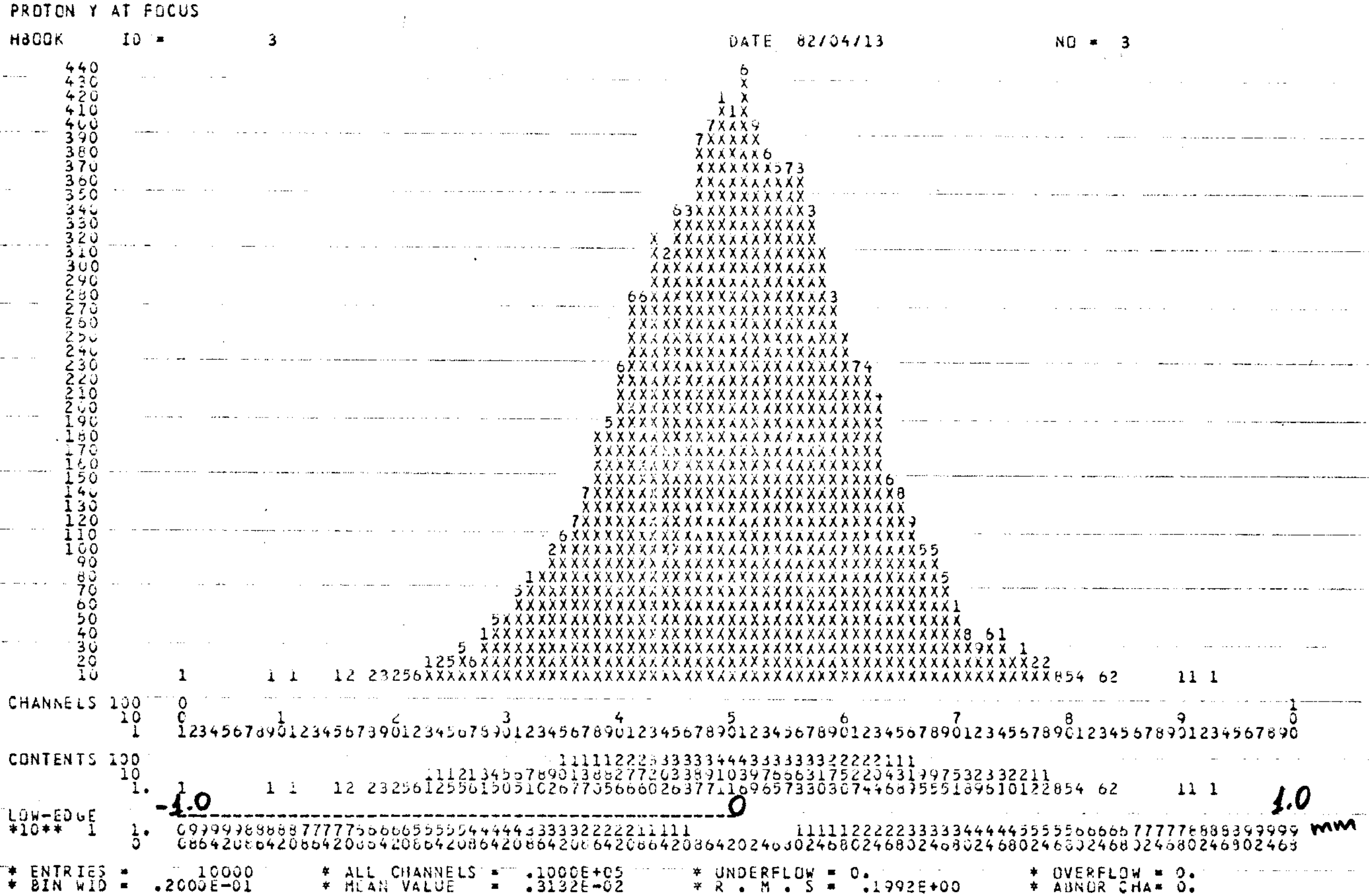


Fig. 9. Proton y - Distribution in the center of the Target ( focus )

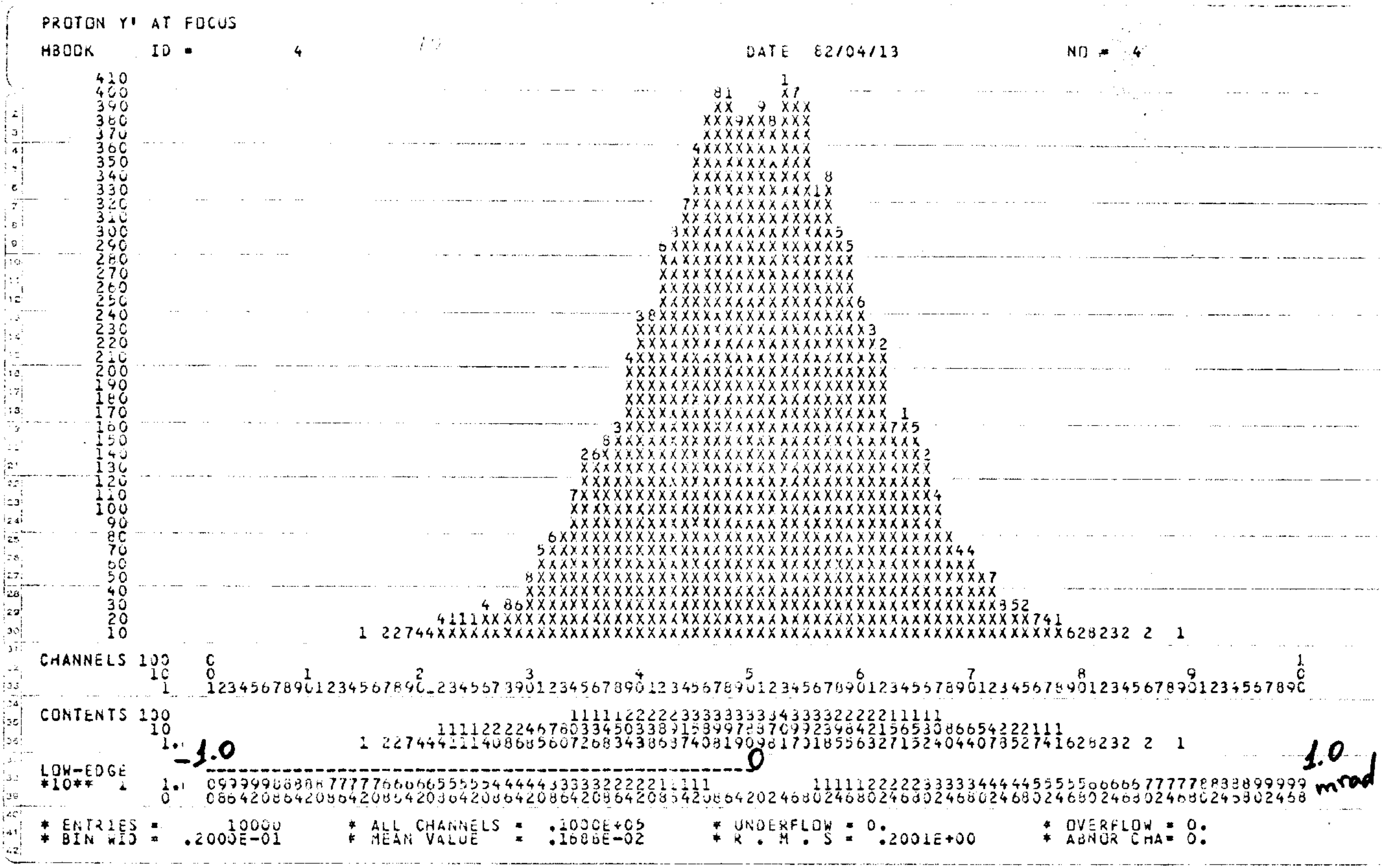


Fig. 10. Proton y' - Distribution in the center of the Target ( Focus )

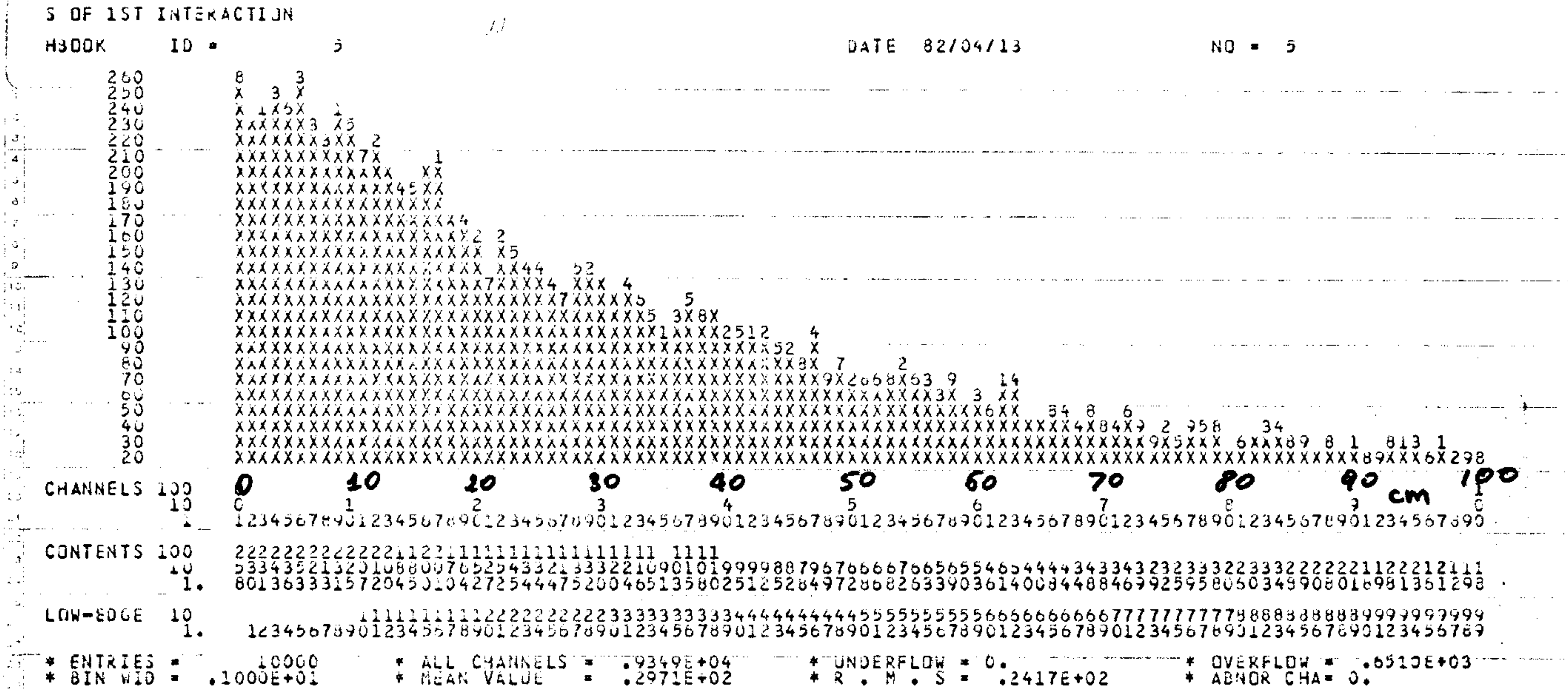


Fig. 11. Distribution of the Decay Distances of the Protons in $\pi^0$'s

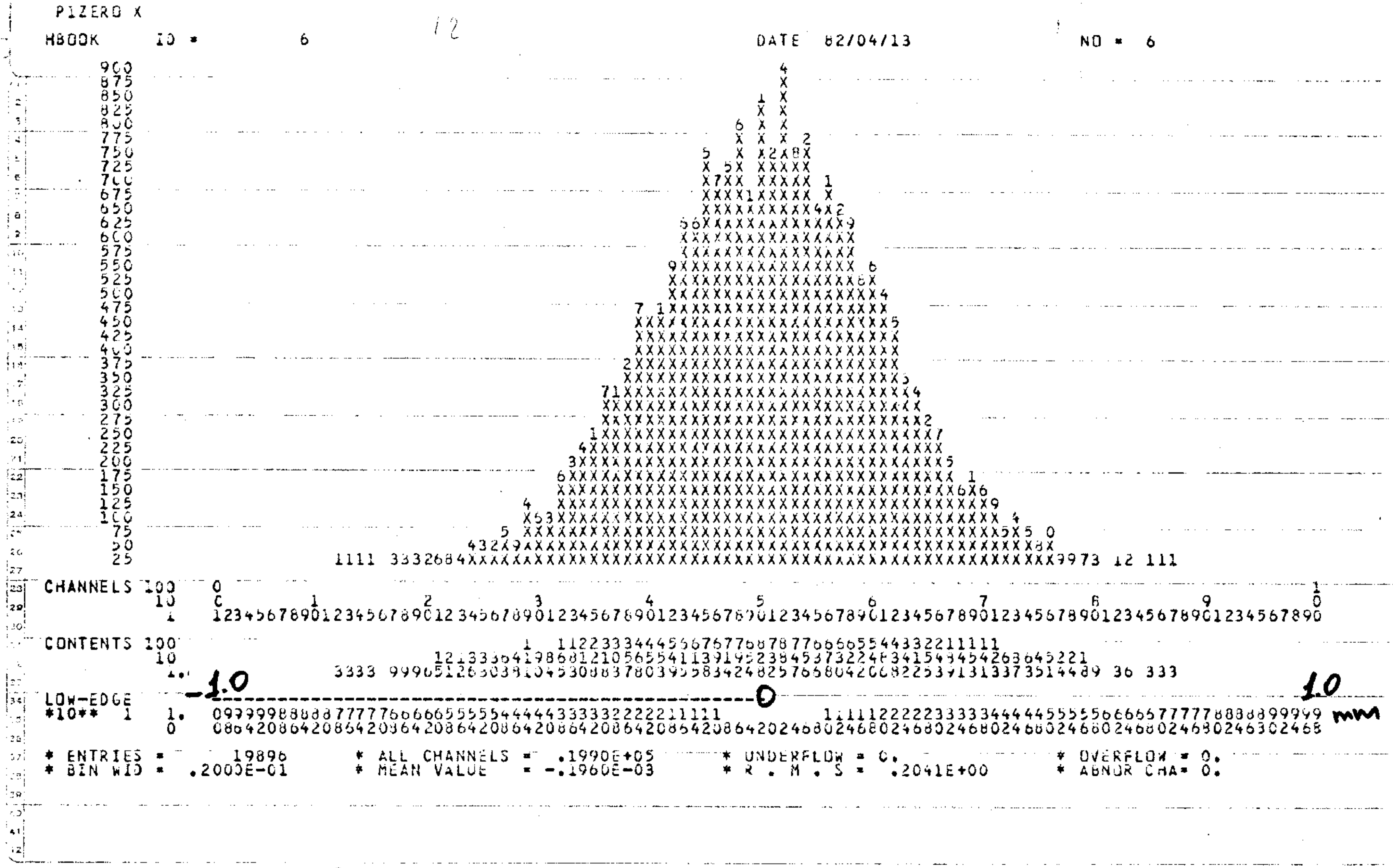


Fig. 12. $\pi^0$ x - Distribution at the moment of production

PIZERO X'

HBOOK ID = 7 DATE 82/04/13 NO = 7

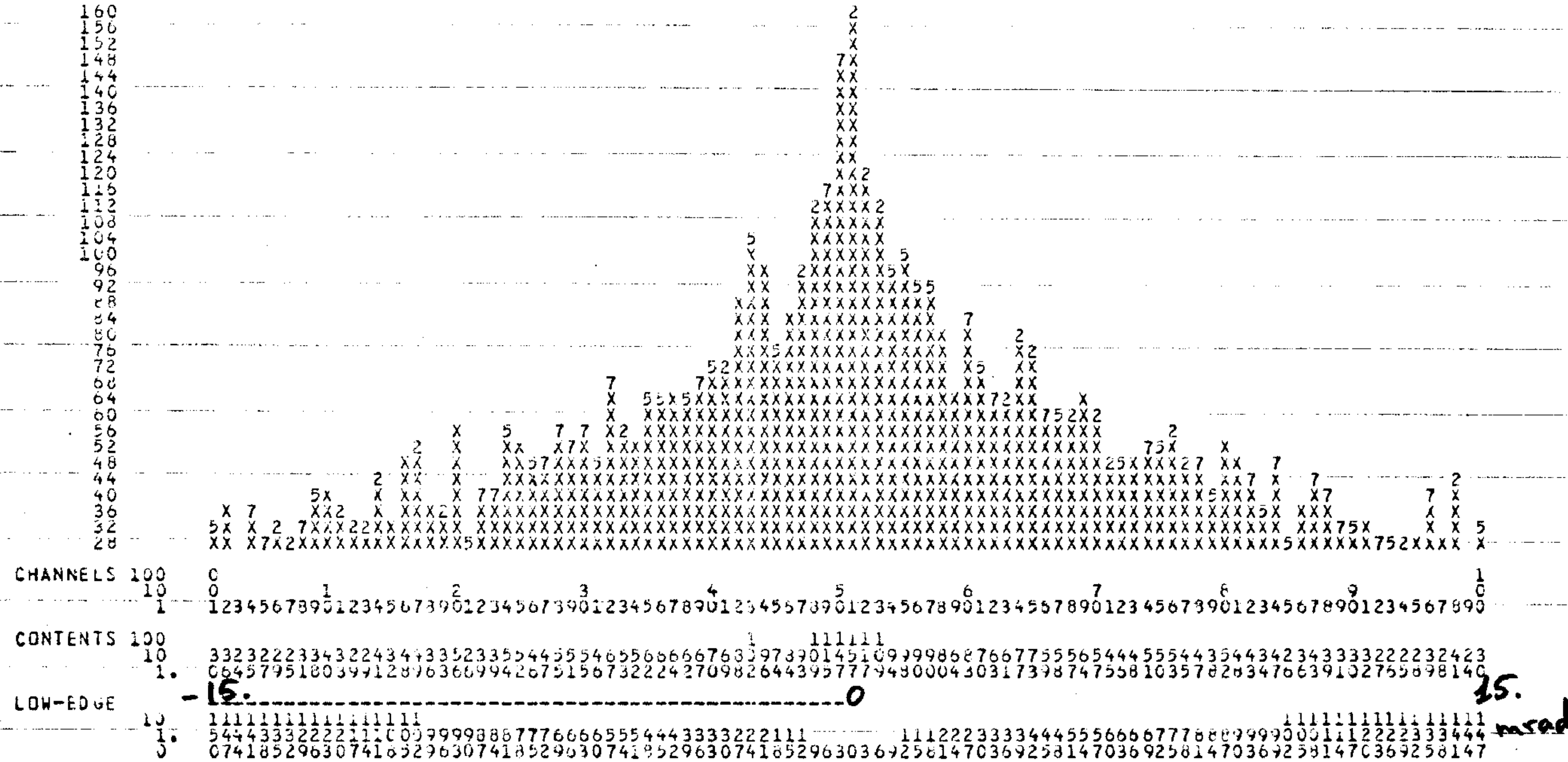


| | | | |
|---|---|---|---|
| * ENTRIES = 19896 | * ALL CHANNELS = .5520E+04 | * UNDERFLOW = .7170E+04 | * OVERFLOW = .7206E+04 |
| * BIN WID = .3000E+00 | * MEAN VALUE = .2717E-02 | * R . M . S = .7101E+01 | * ABNOR CHA= 0. |

Fig. 13. $\pi^0$ x' – Distribution at the moment of production

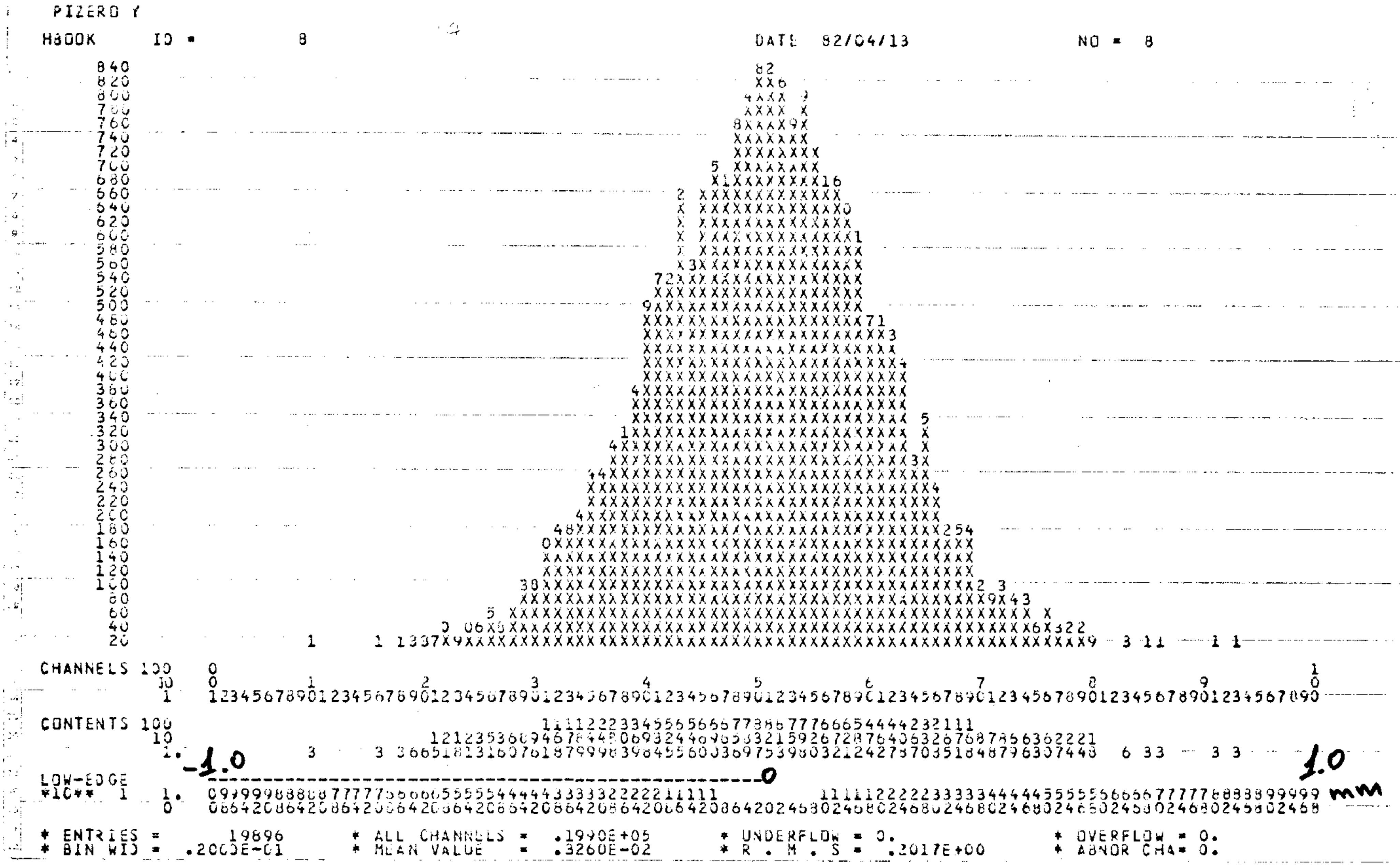


Fig. 14. $\pi^0$ y - Distribution at the moment of production

PIZERO Y'

HBOOK ID = 9 DATE 82/04/13 NO = 9

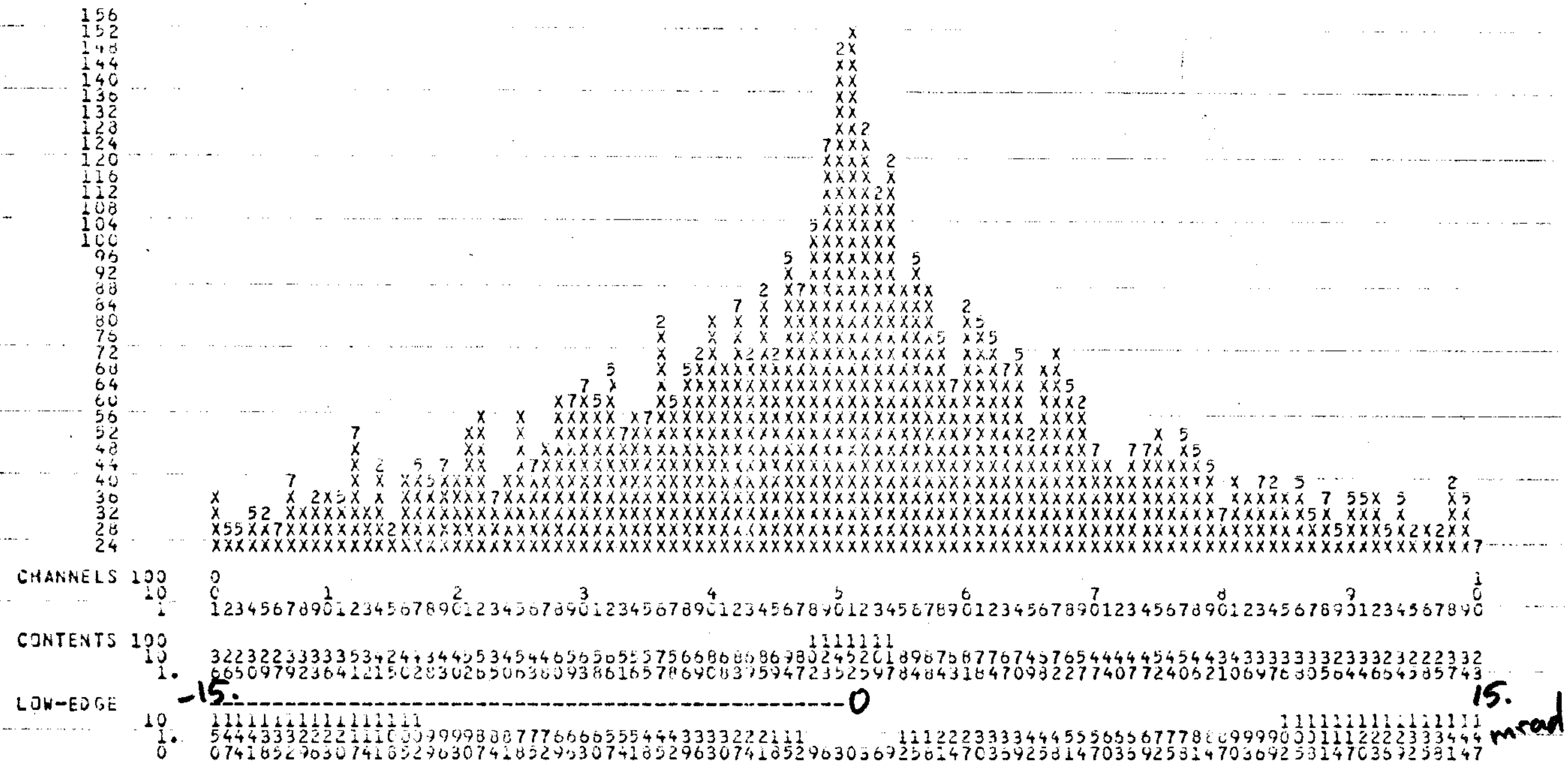


* ENTRIES = 19896 * ALL CHANNELS = .5504E+04 * UNDERFLOW = .7267E+04 * OVERFLOW = .7125E+04
* BIN WID = .3000E+00 * MEAN VALUE = -.1707E+00 * R . M . S = .7097E+01 * ABNOR CHA= 0.

Fig. 15. $\pi^0$ y' - Distribution at the moment of production

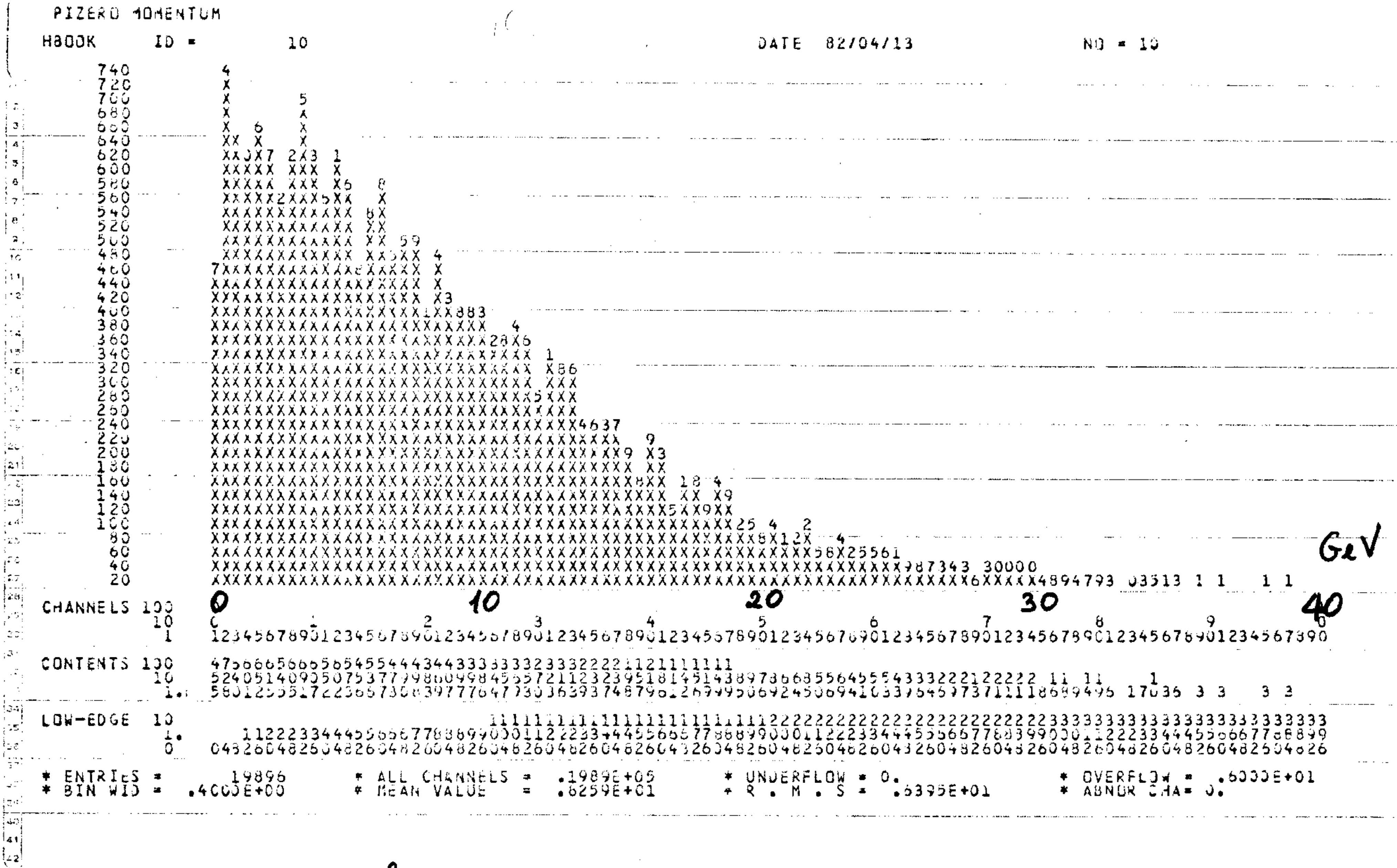


Fig. 16. $\pi^0$ Momentum Distribution at the moment of production

GAMMA1 X'

HBOOK ID = 11 DATE 82/04/13 NO = 11

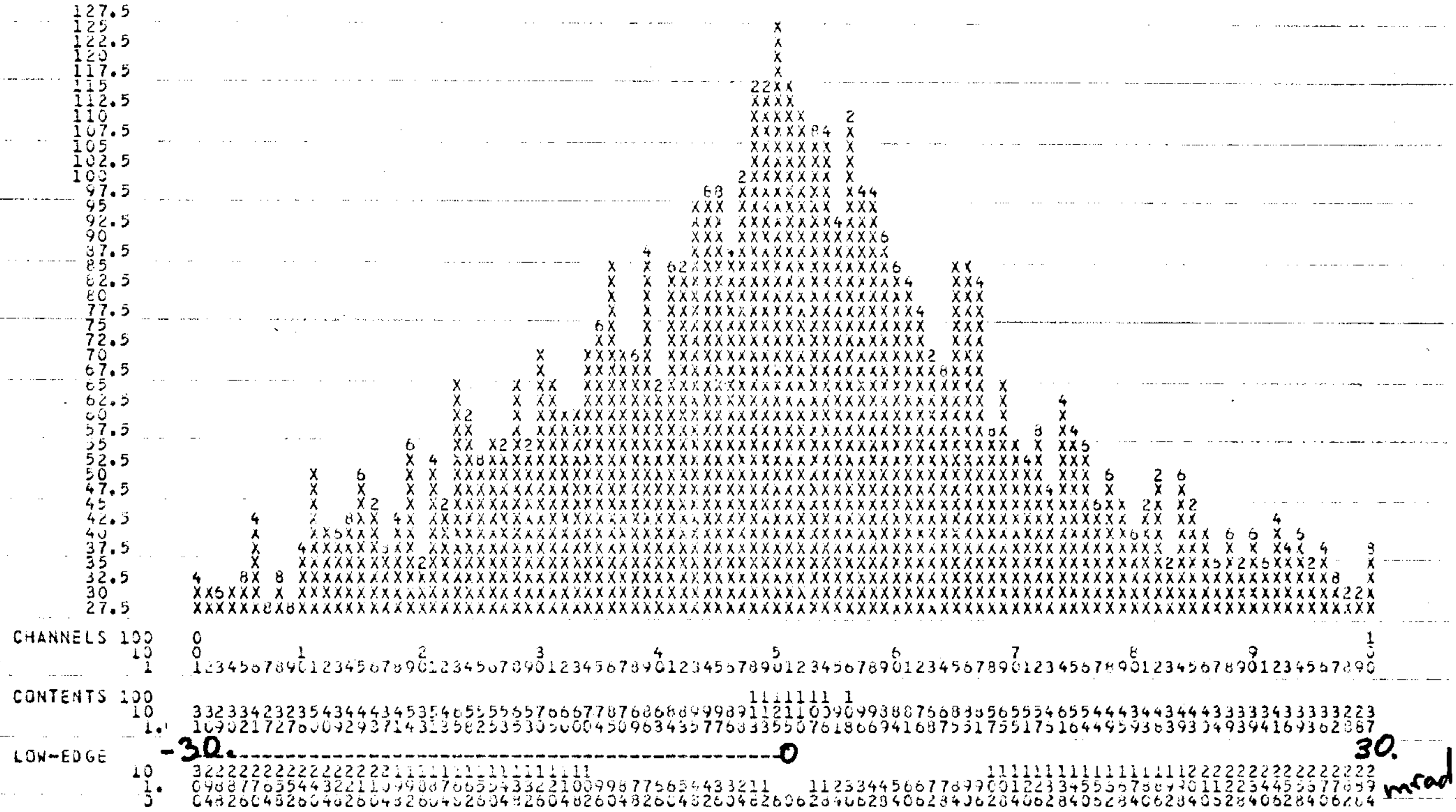


* ENTRIES = 19896 * ALL CHANNELS = .5970E+04 * UNDERFLOW = .6933E+04 * OVERFLOW = .6983E+04
* BIN WID = .6000E+00 * MEAN VALUE = -.1018E+00 * R . M . S = .1432E+02 * ABNOR CHA = 0.

Fig. 17. x' - Distribution of gamma #1 at $\pi^0$ decay

GAMMA1 Y'

HBOOK ID = 12 DATE 82/04/13 NO = 12

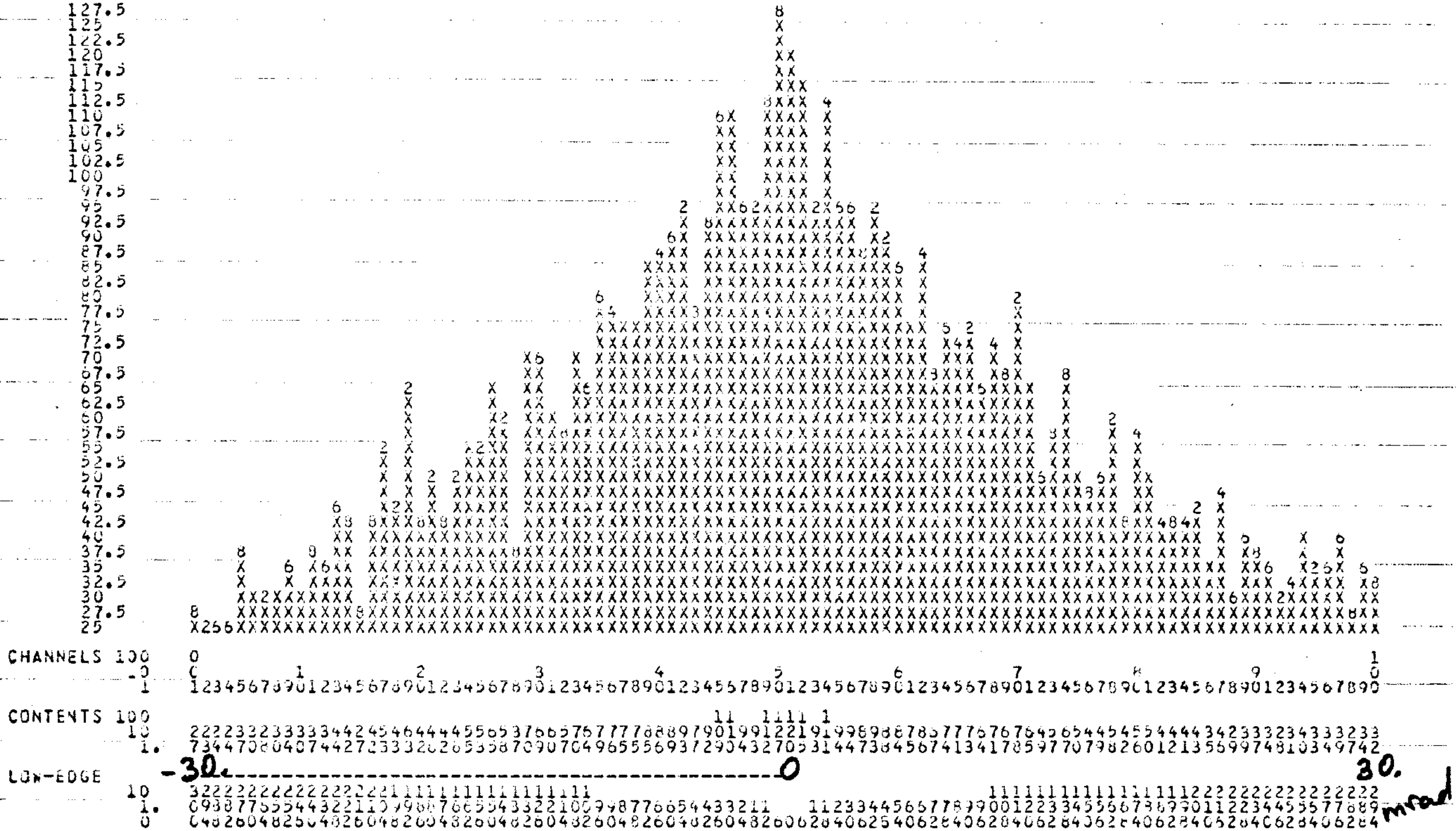


* ENTRIES = 19896 * ALL CHANNELS = .5962E+04 * UNDERFLOW = .6980E+04 * OVERFLOW = .6954E+04
* BIN WID = .6000E+00 * MEAN VALUE = .1349E+00 * R . M . S = .1417E+02 * ABNOR CHA= 0.

Fig. 18. y' - Distribution of gamma #1 at $\pi^0$ decay

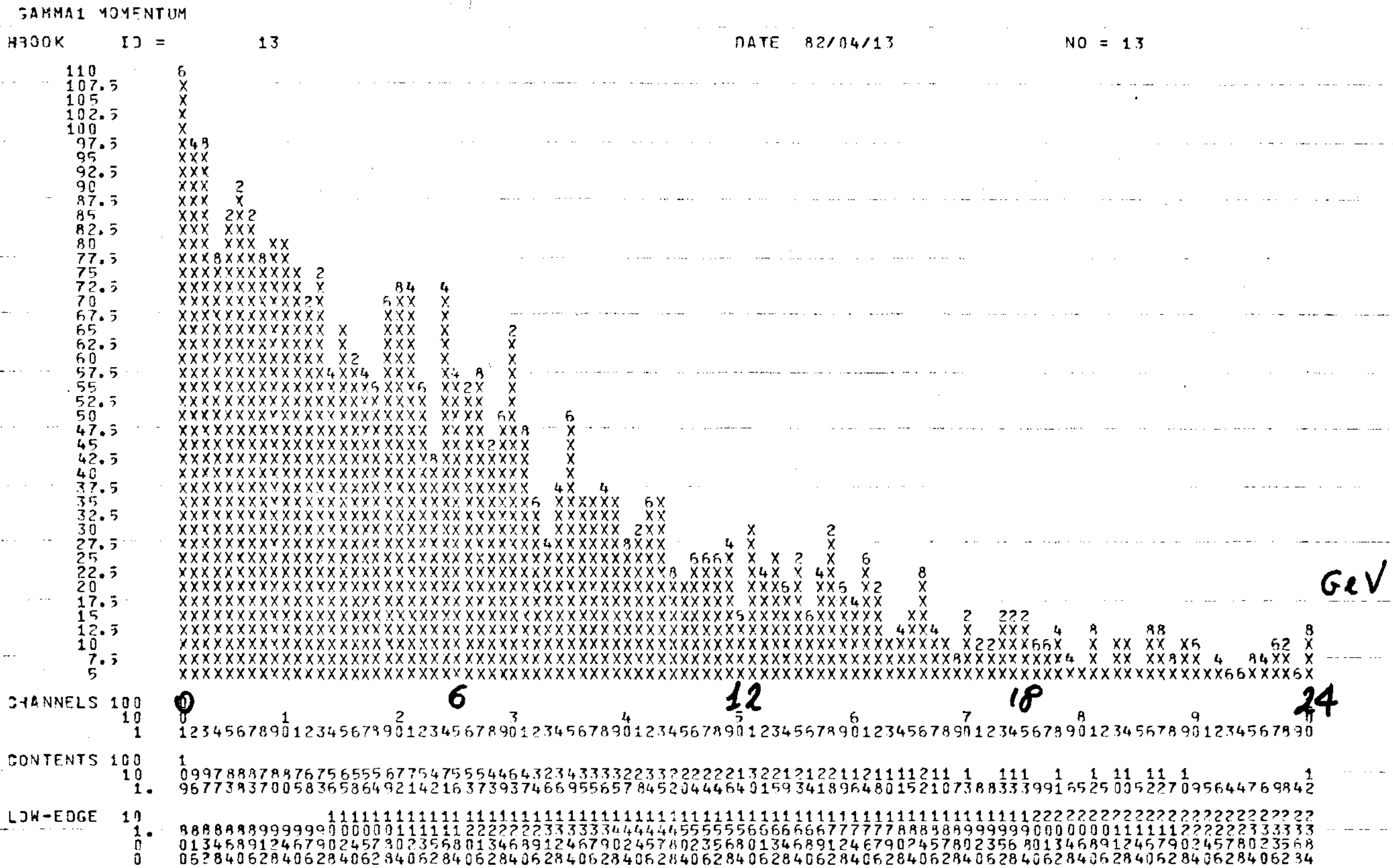


Fig. 19. Momentum Distribution of gamma #1 at $\pi^0$ decay

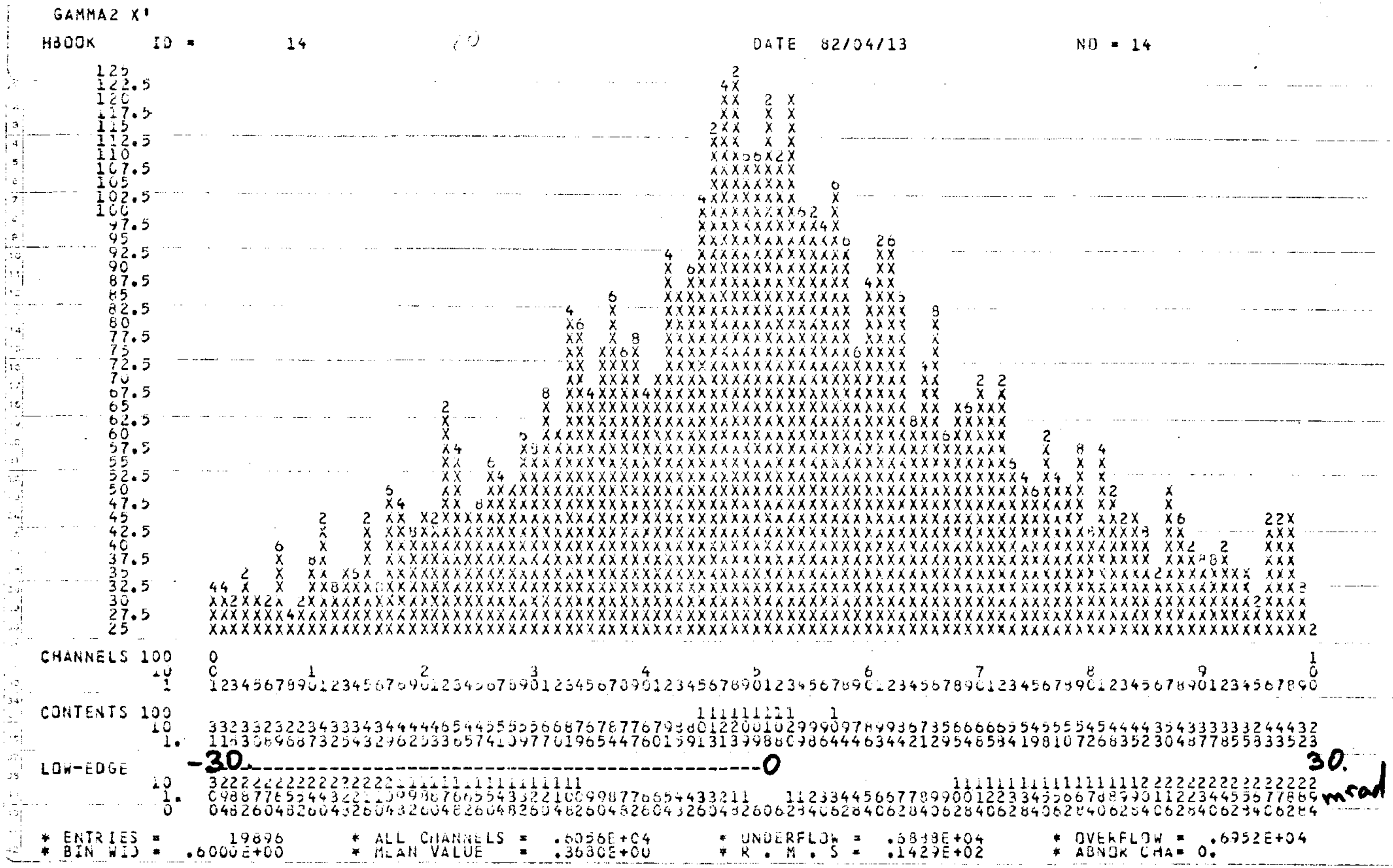


Fig. 20. x' - Distribution of gamma #2 at $\pi^0$ decay

GAMMA2 Y'

HBOOK ID = 15 DATE 82/04/13 NO = 15

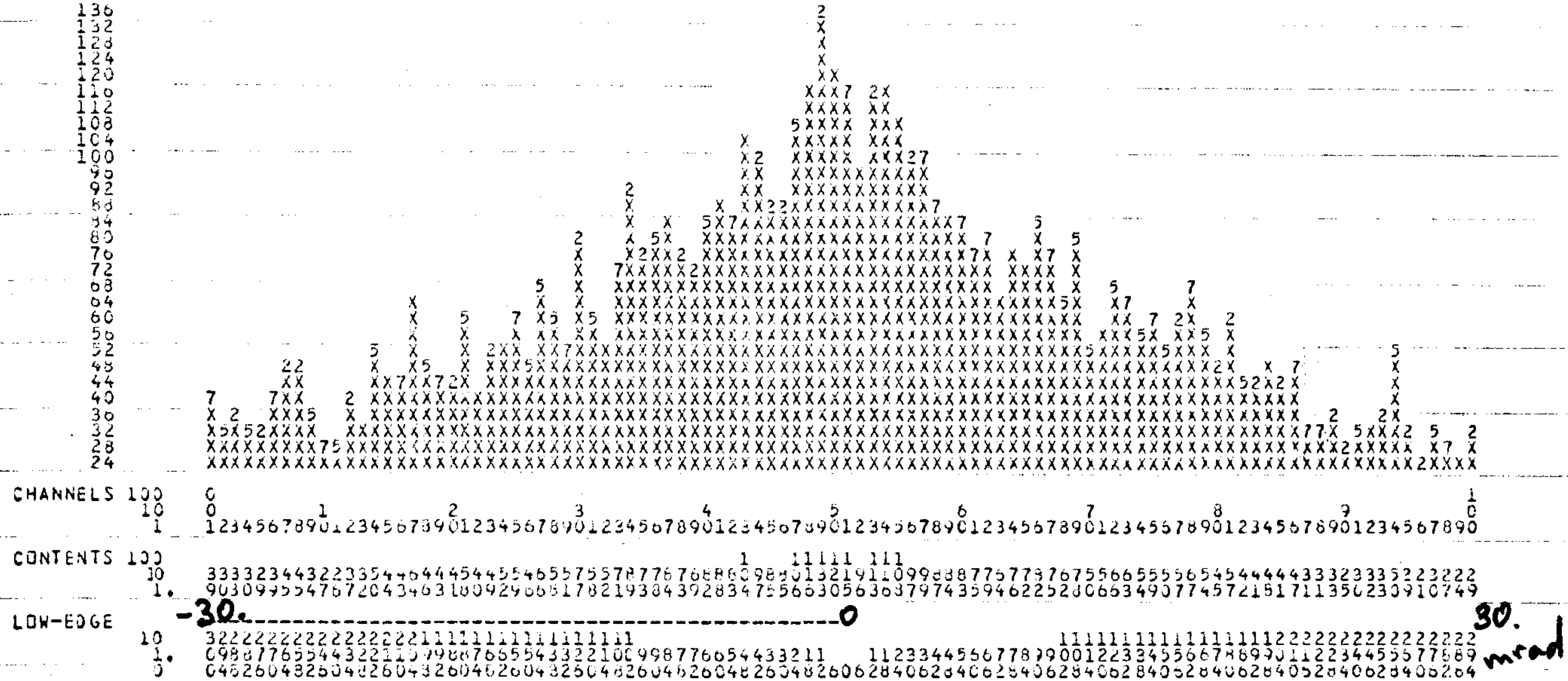


* ENTRIES = 19896 * ALL CHANNELS = .6062E+04 * UNDERFLOW = .5938E+04 * OVERFLOW = .6895E+04

* BIN WID = .6000E+00 * MEAN VALUE = -.2982E+00 * R . M . S = .1421E+02 * ABNOR CHA= 0.

Fig. 21. y' - Distribution of gamma #2 at $\pi^0$ decay

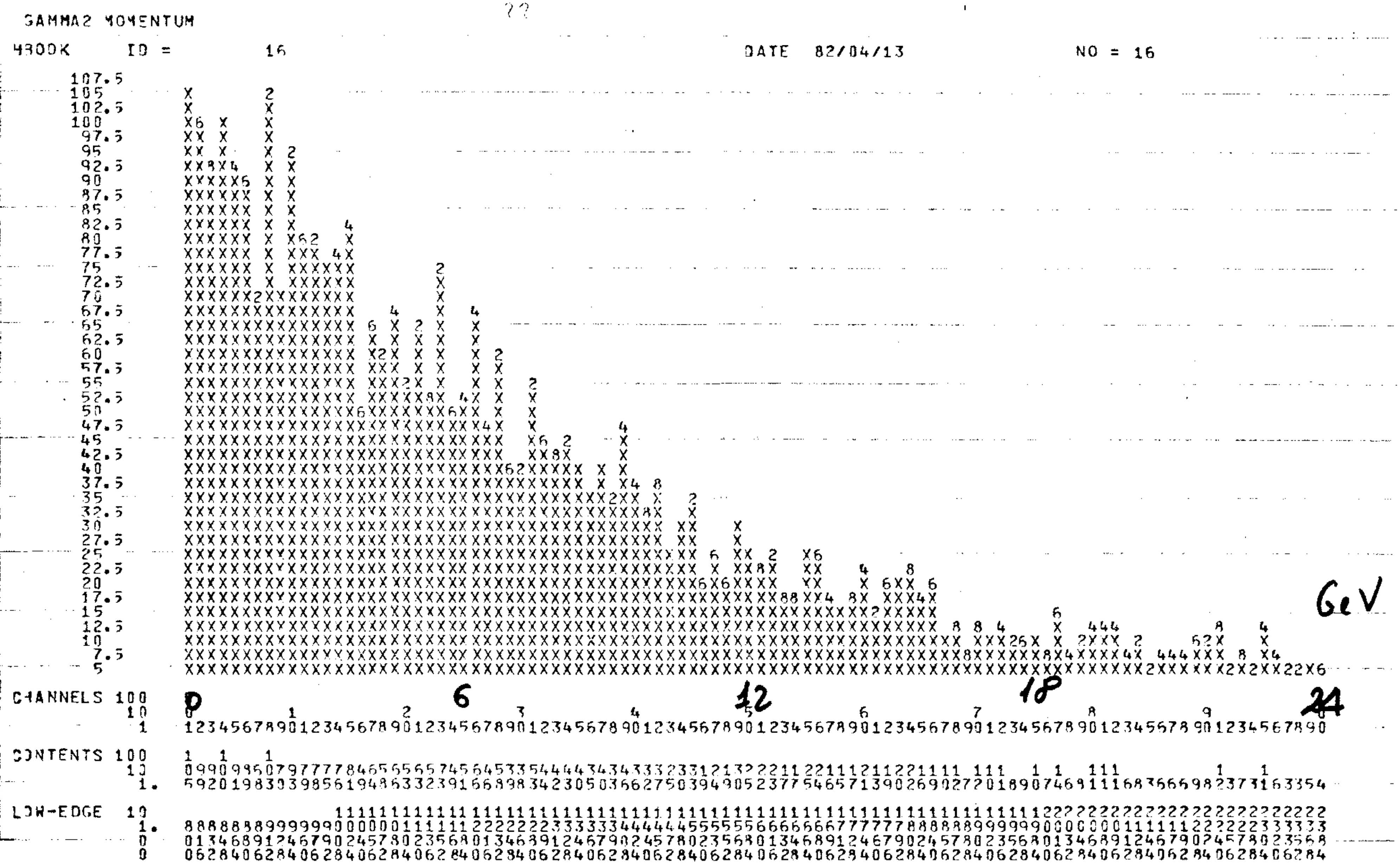


* ENTRIES = 19896 * ALL CHANNELS = .3382E+04 * UNDERFLOW = .1640E+05 * OVERFLOW = .1170E+03

Fig. 22. Momentum Distribution of gamma #2 at $\pi^0$ decay

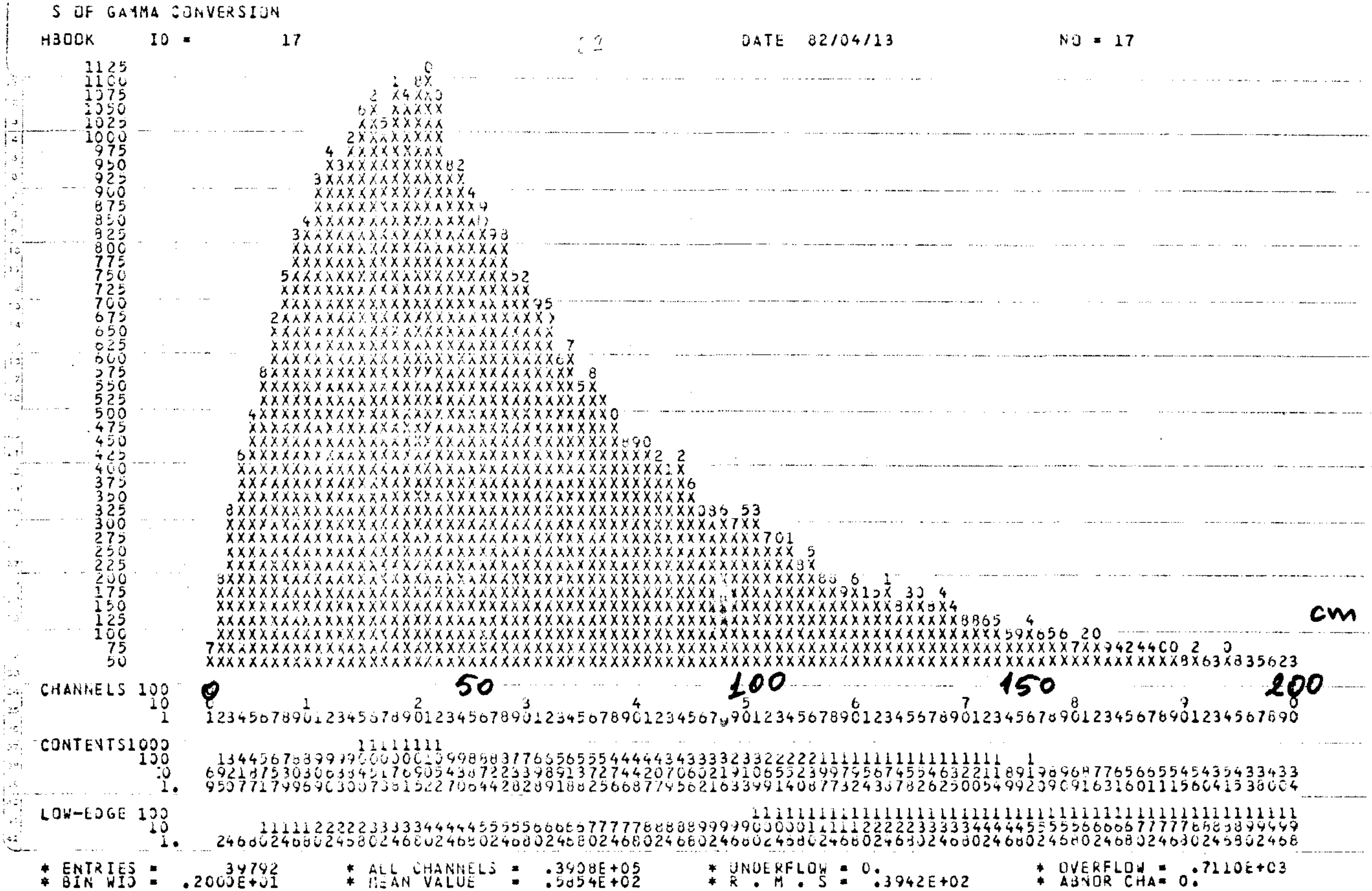


Fig. 23. Distribution of conversion distances for $\gamma \rightarrow e^{+} + e^{-}$

X AT GAMMA CONVERSION

HBOOK ID = 18 DATE 82/04/13 NO = 18

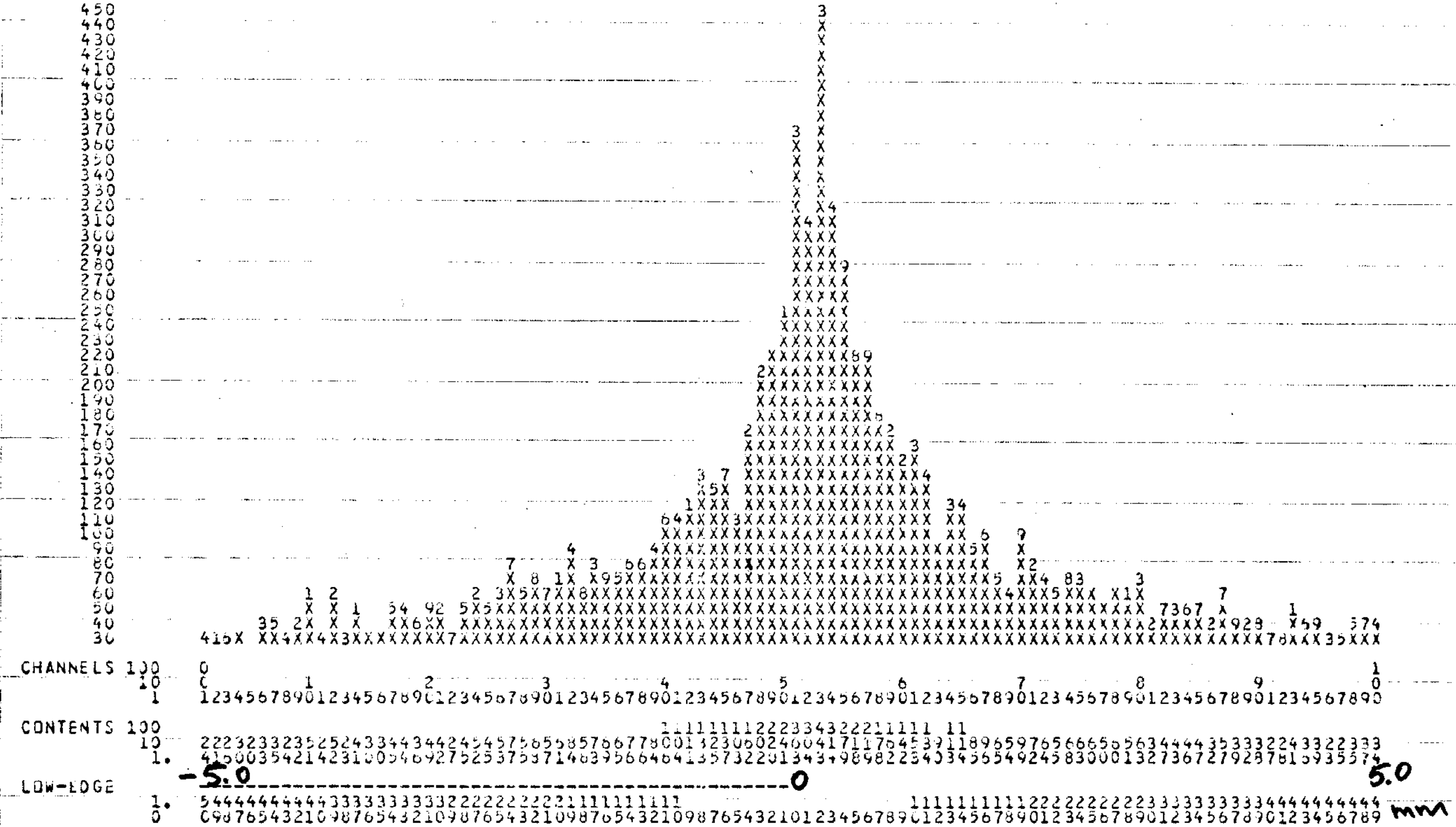


* ENTRIES = 22302 * ALL CHANNELS = .6450E+04 * UNDERFLOW = .6785E+04 * OVERFLOW = .7067E+04
* BIN WID = .1000E+00 * MEAN VALUE = .1532E+00 * R . M . S = .1993E+01 * ABNOR CHA= 0.

Fig. 24. x - Distribution at gamma conversion

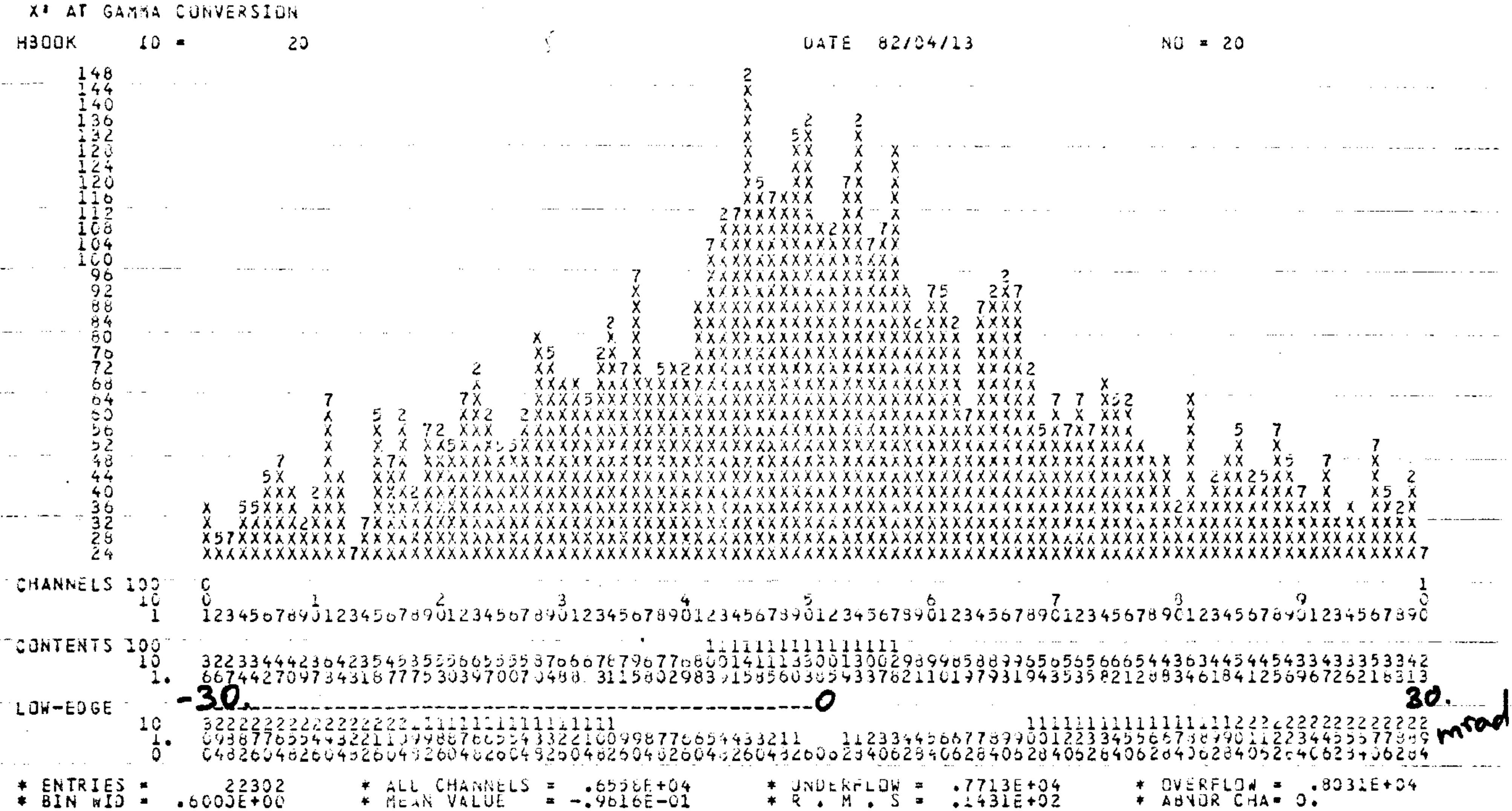


Fig. 25. x' - Distribution at gamma conversion

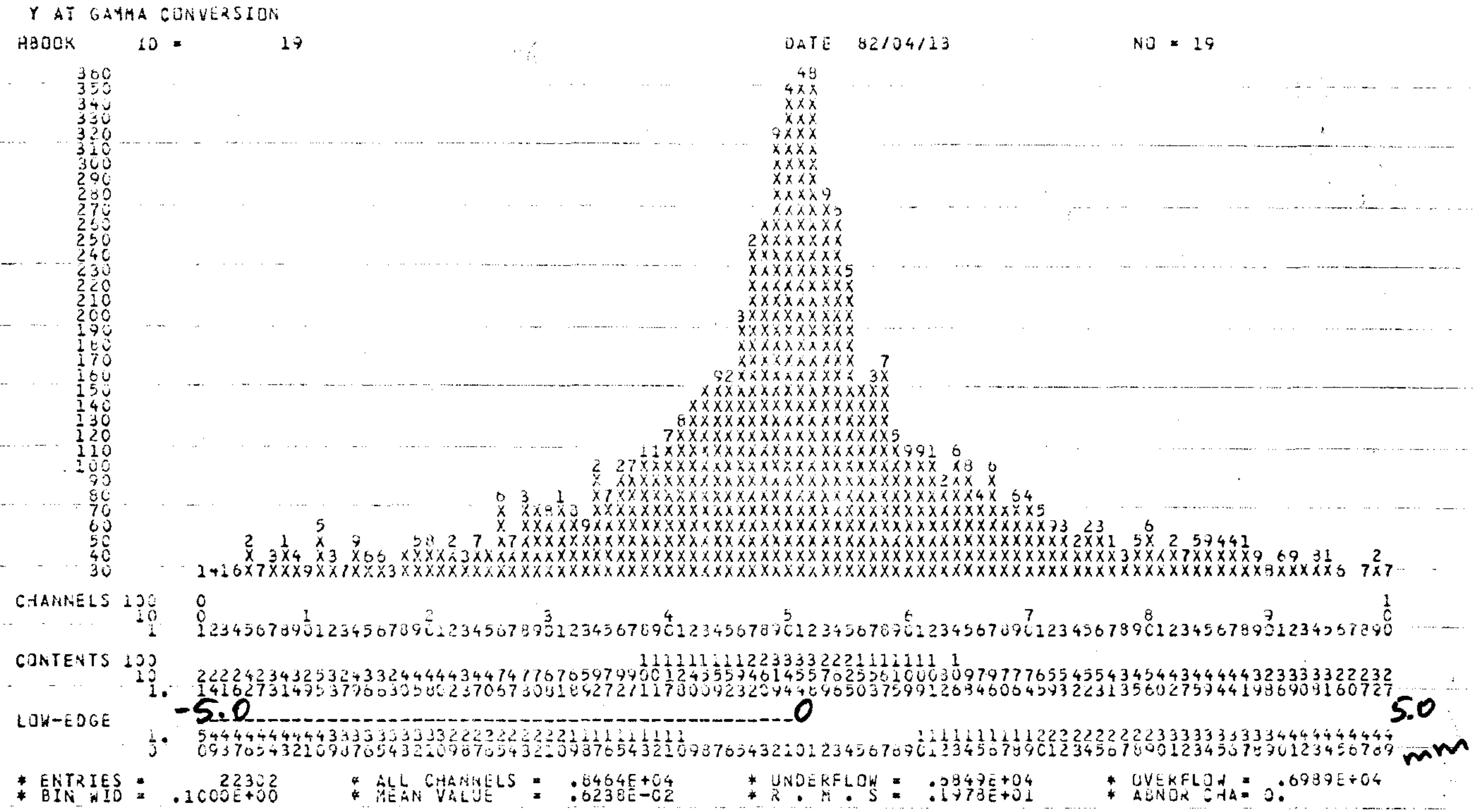


Fig. 26. y - Distribution at gamma conversion

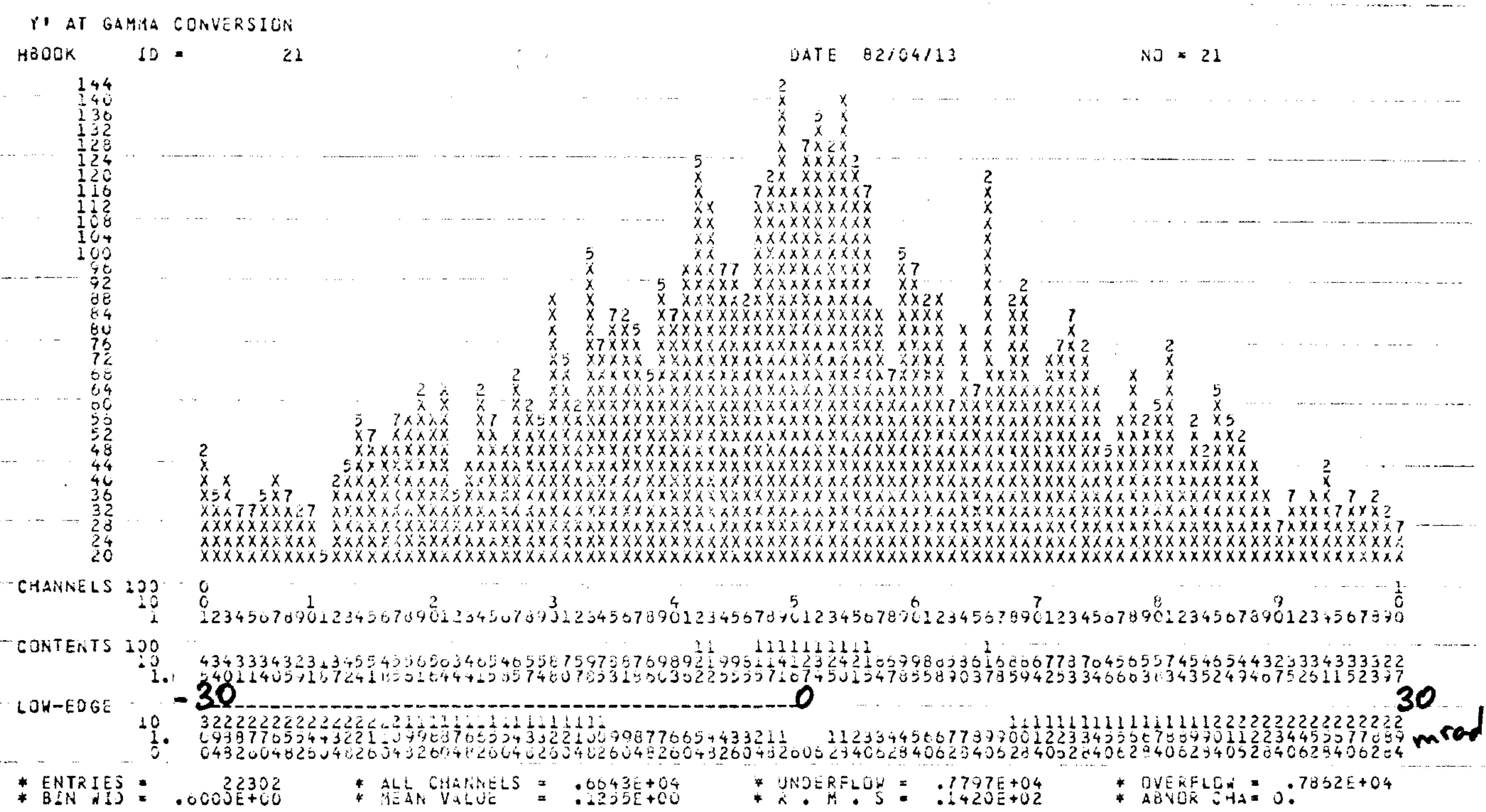


Fig. 27. y' - Distribution at gamma conversion

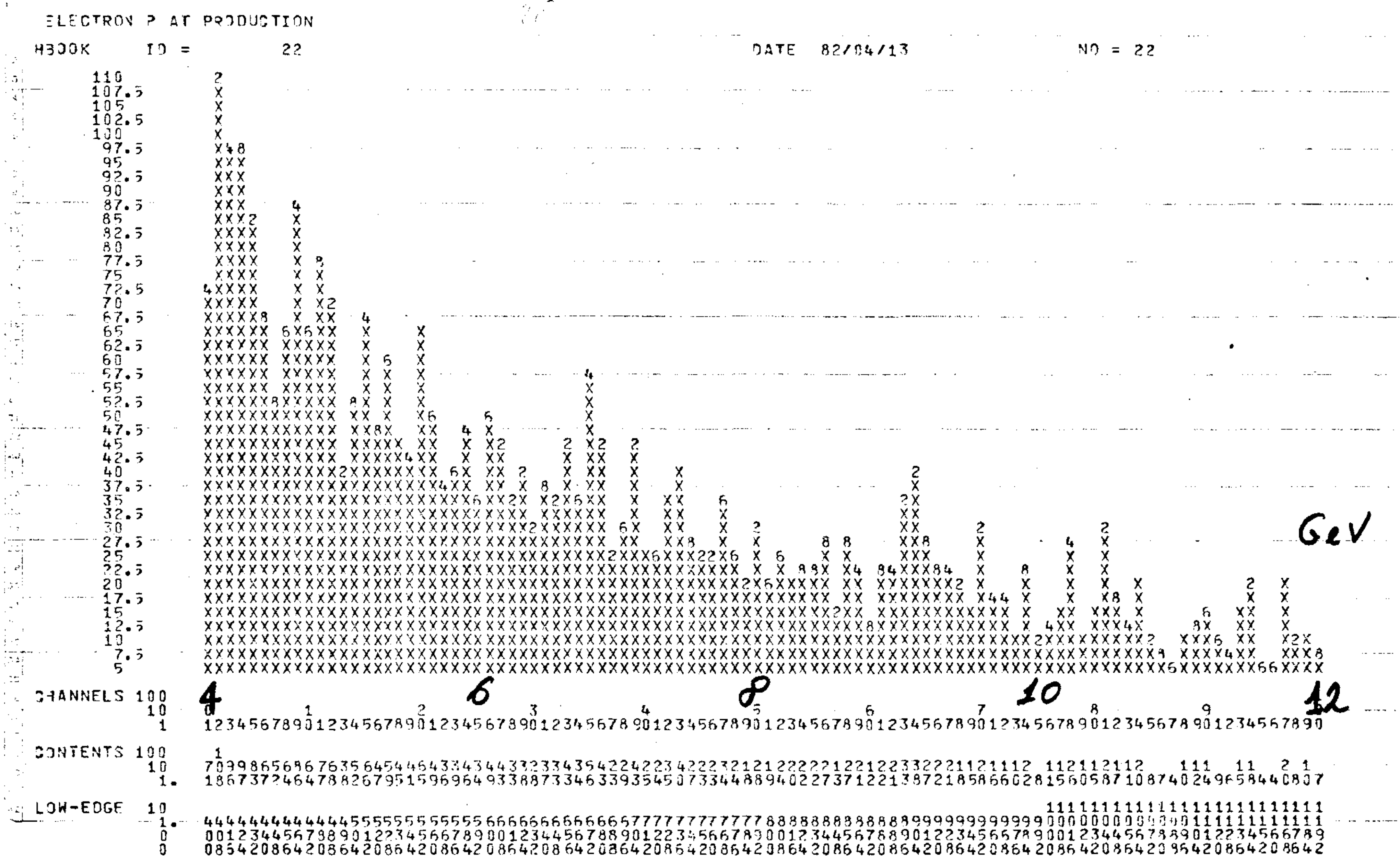


Fig. 28. Momentum Distribution of the Electrons at conversion

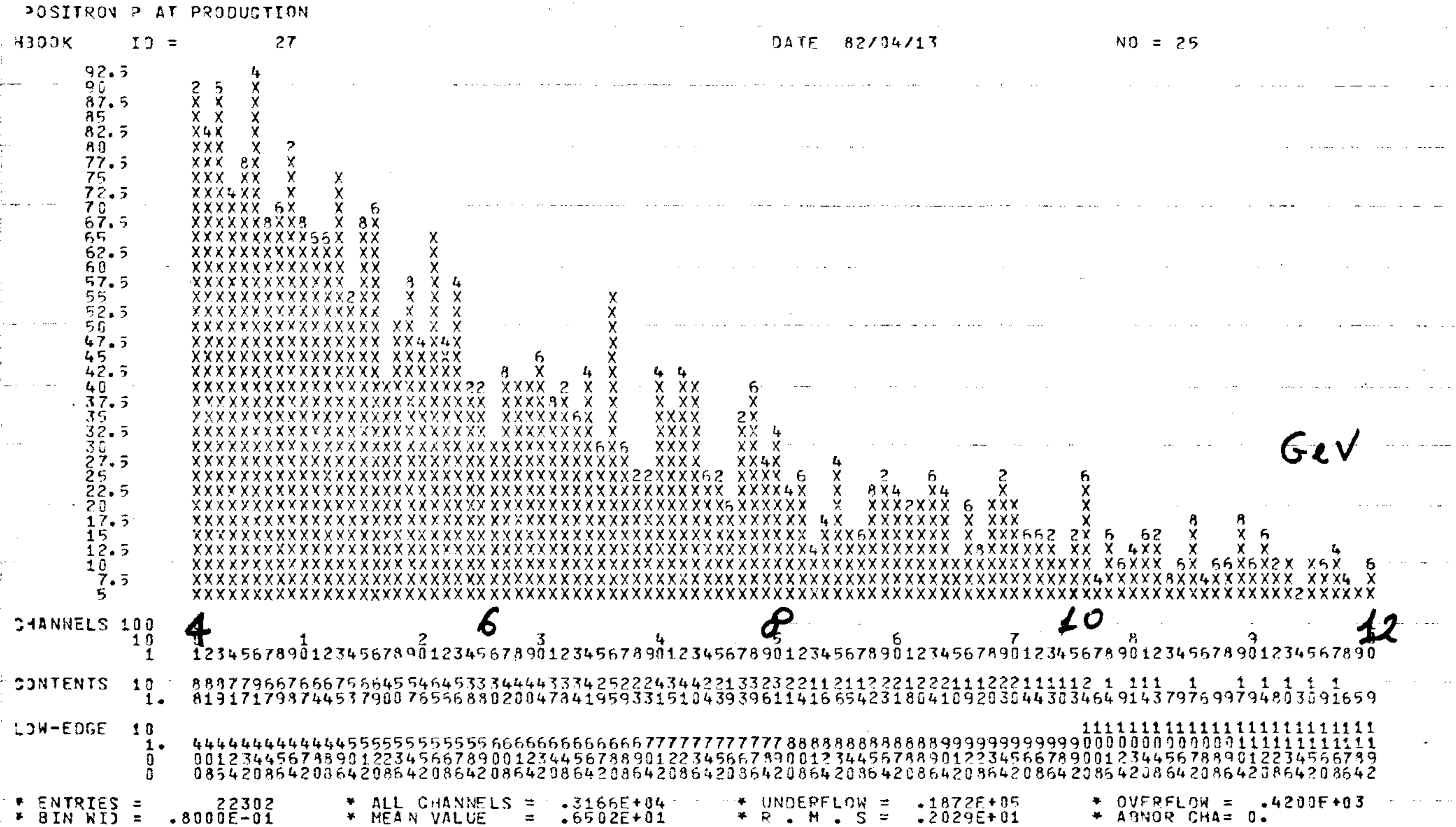


Fig. 29. Momentum Distribution of the Positrons at conversion

S OF E- BREMSSTR.

HBOOK ID = 23 DATE 82/04/13 NO = 23

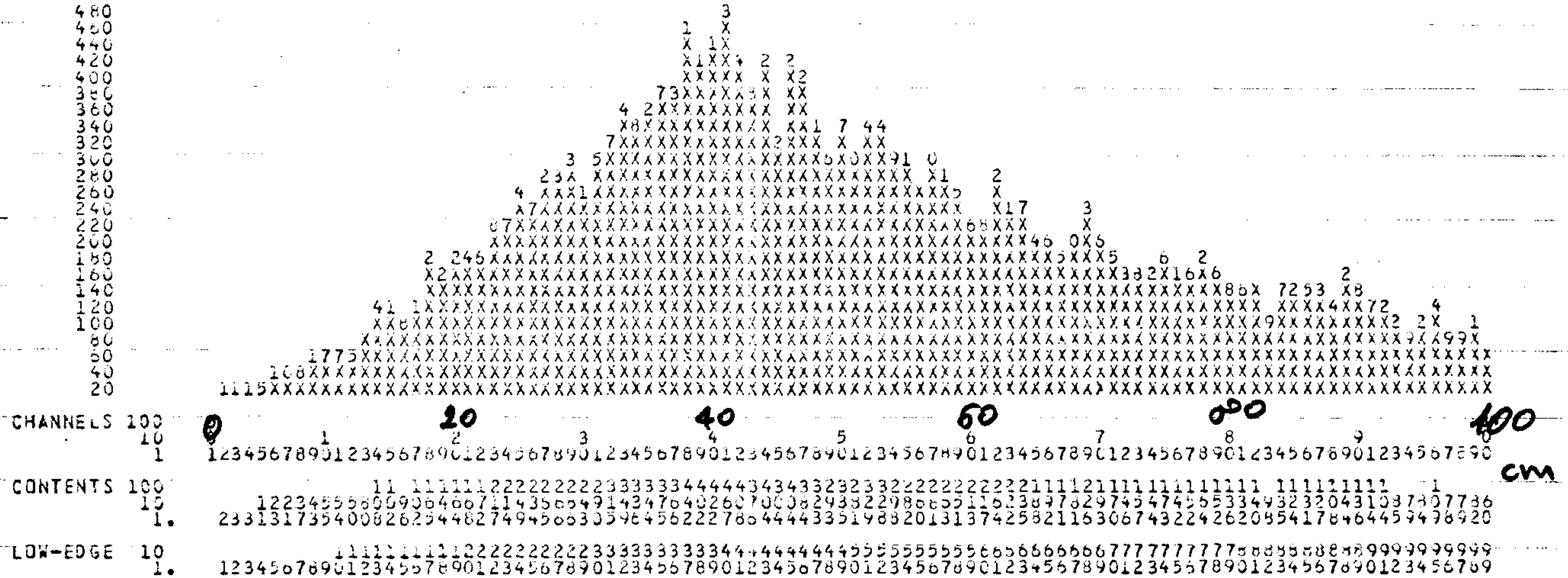


* ENTRIES = 22302 * ALL CHANNELS = .1948E+05 * UNDERFLOW = 0. * OVERFLOW = .2826E+04
* BIN WID = .1000E+01 * MEAN VALUE = .4956E+02 * R . M . S = .2127E+02 * ABNOR CHA = 0.

Fig. 30. Distribution of Bremmstrahlung Distances for Electrons

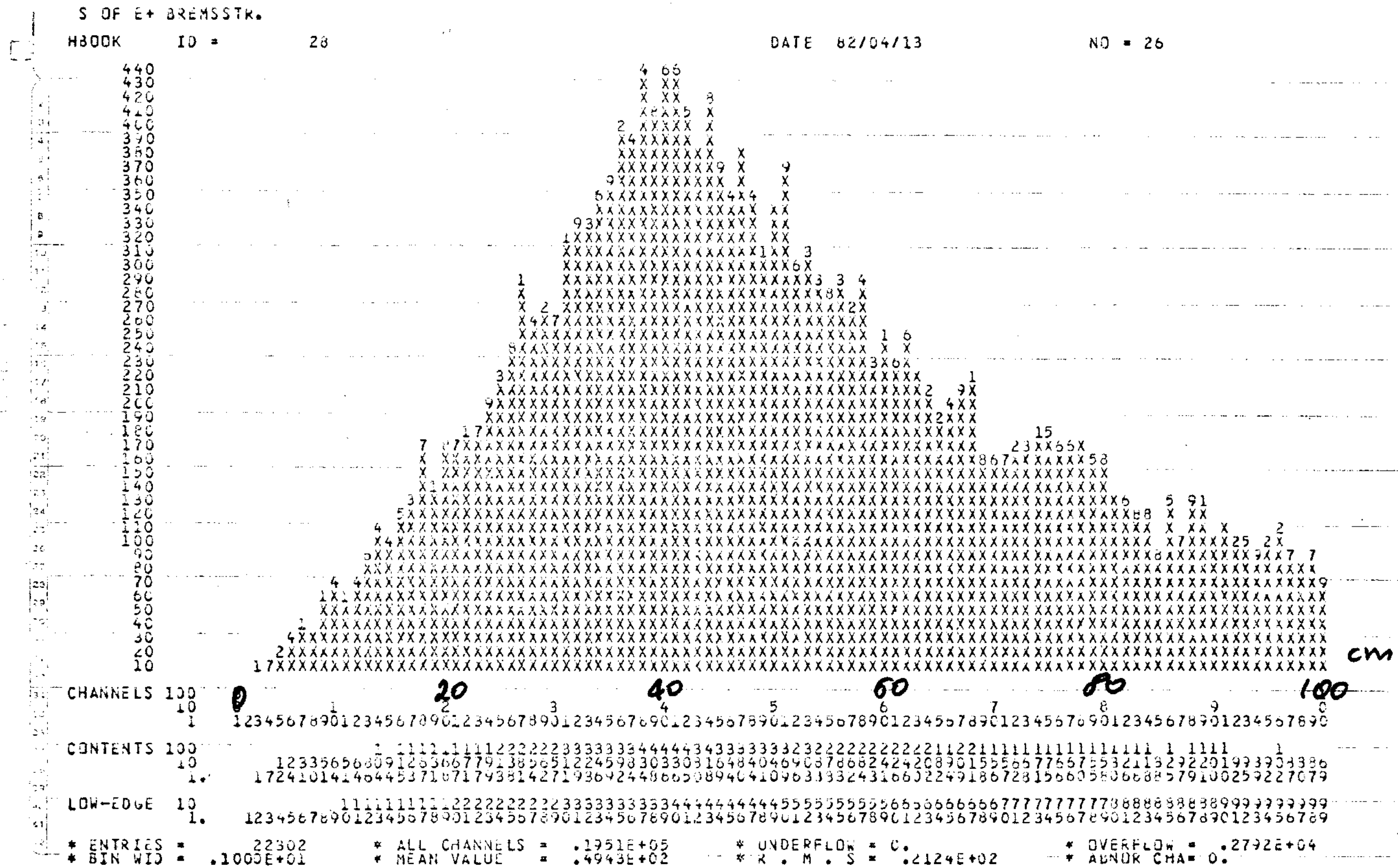


Fig. 31. Distribution of Bremmstrahlung Distances for Positrons

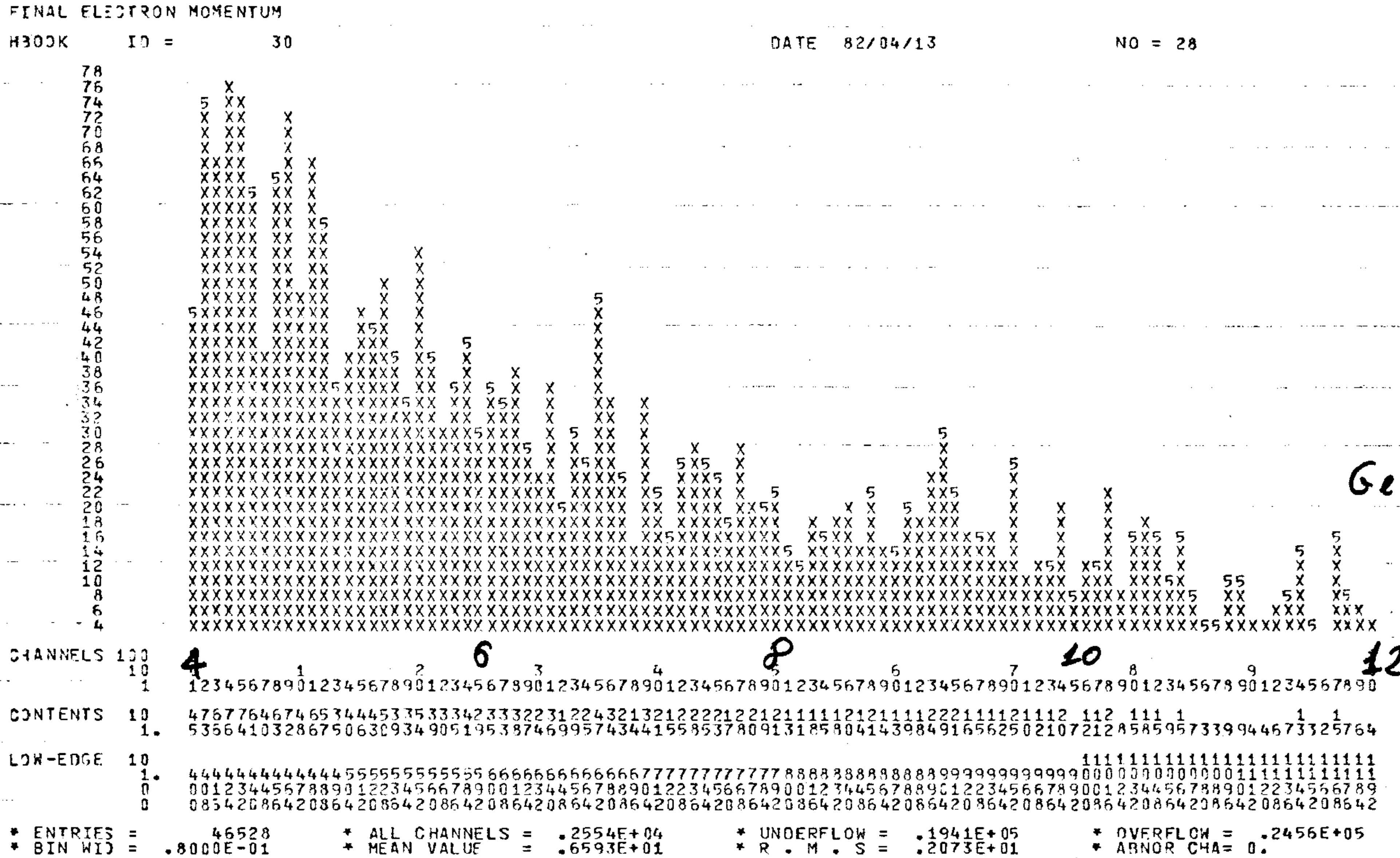


Fig. 32. Final Momentum Distribution for the Electrons

FINAL POSITRON MOMENTUM

HBOOK ID = 31 DATE 82/04/13 NO = 29

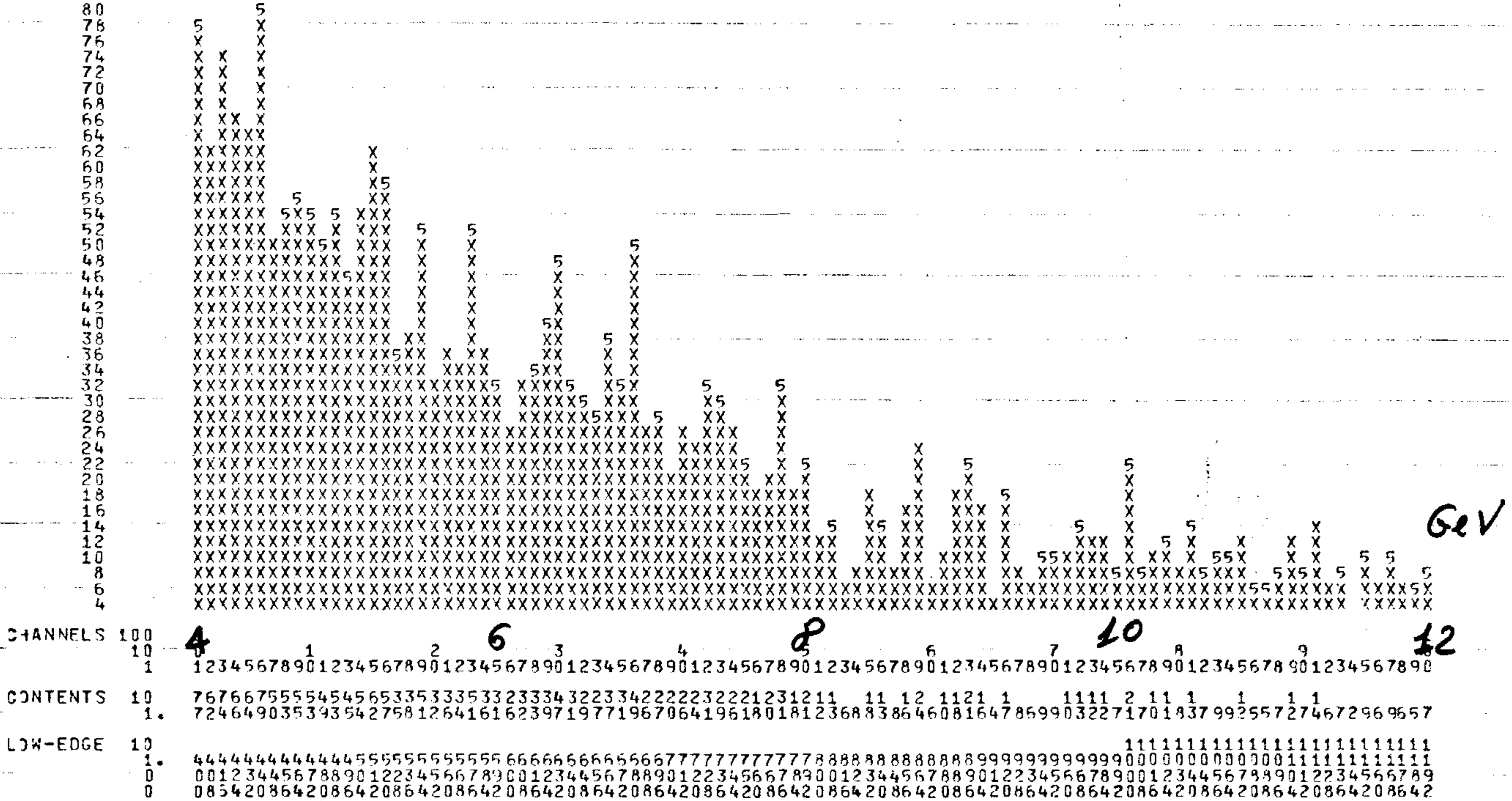


* ENTRIES = 46528 * ALL CHANNELS = .2526E+04 * UNDERFLOW = .1947E+05 * OVERFLOW = .2454E+05
* BIN WID = .8000E-01 * MEAN VALUE = .6442E+01 * R . M . S = .2013E+01 * ABNOR CHA= 0.

Fig. 33. Final Momentum Distribution for the Positrons

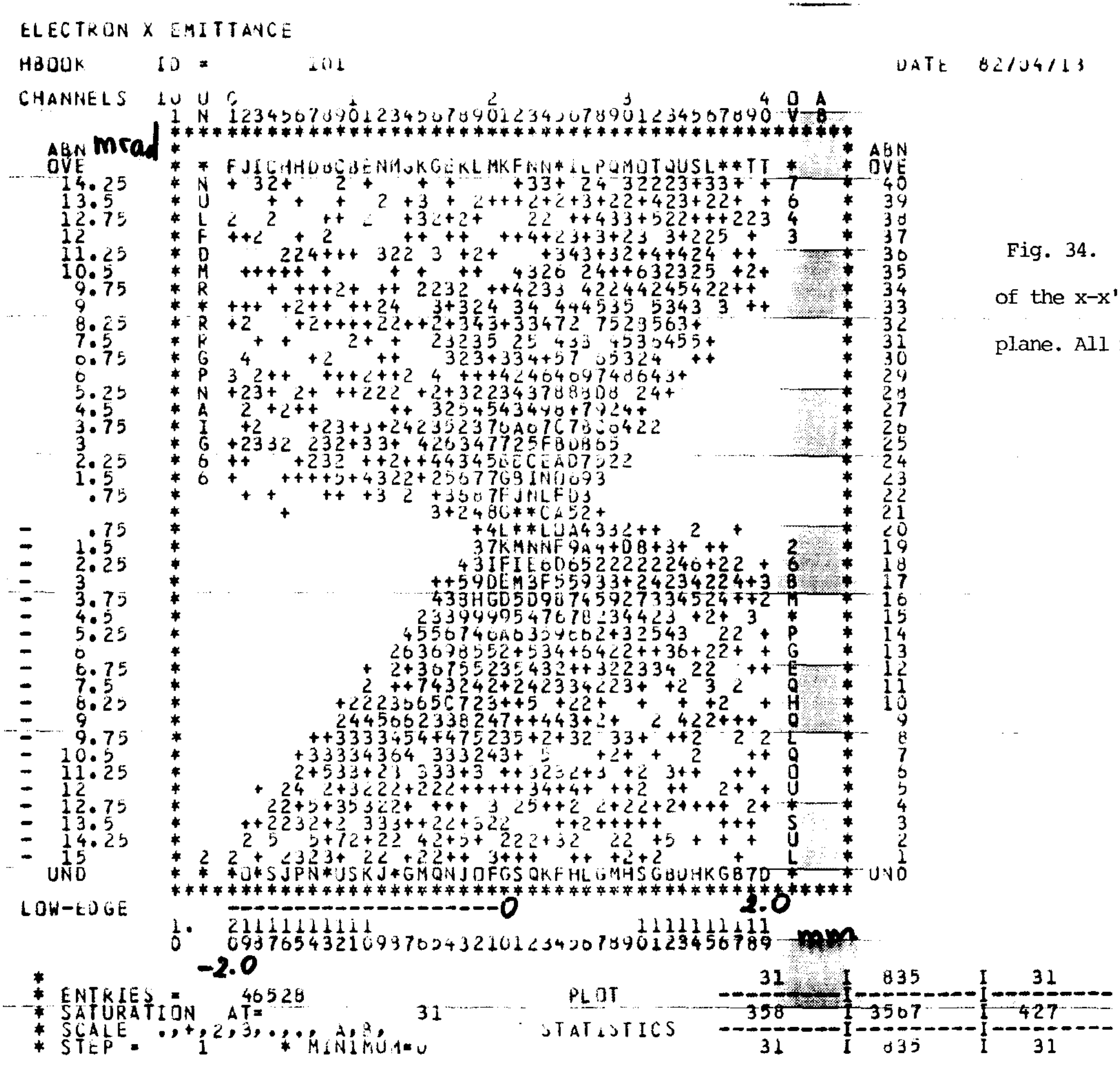


Fig. 34. Electron Population of the x-x' phase space at the focal plane. All momenta are included

ELECTRON Y EMITTANCE

HBOOK ID = 102 DATE 82/04/13 NO = 31

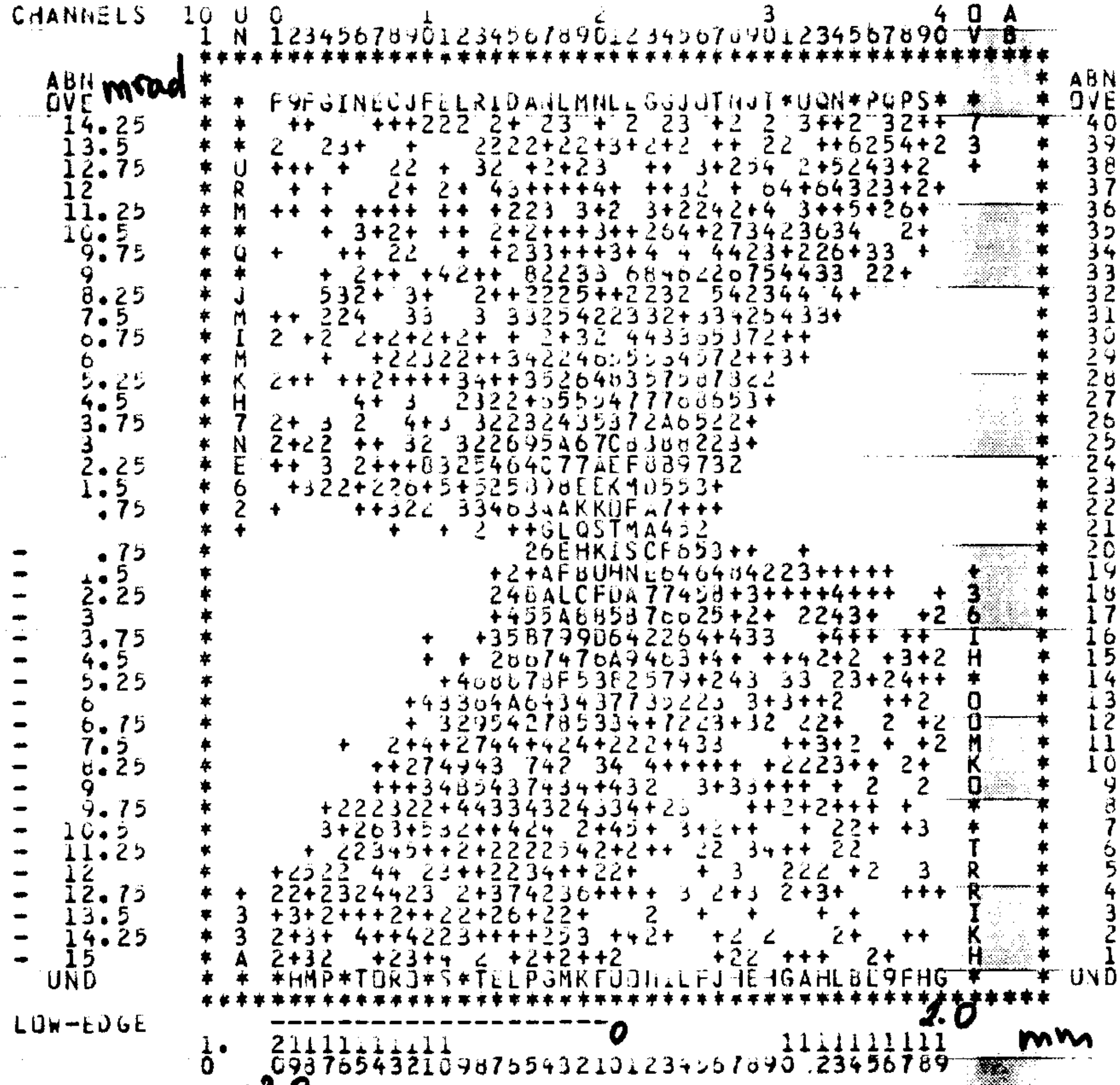


* ENTRIES = 46526
* SATURATION AT= 31
* SCALE .,+,2,3,.,.,., A,B,
* STEP = 1 * MINIMUM=0

PLOT STATISTICS

| | | |
|---|---|---|
| 31 | 841 | 31 |
| 417 | 3614 | 401 |
| 31 | 832 | 31 |

Fig. 35. Electron Population of the y-y' phase space at the focal plane. All momenta are included

POSITRON X EMITTANCE

HBOOK ID = 103 DATE 82/04/13 NO = 32

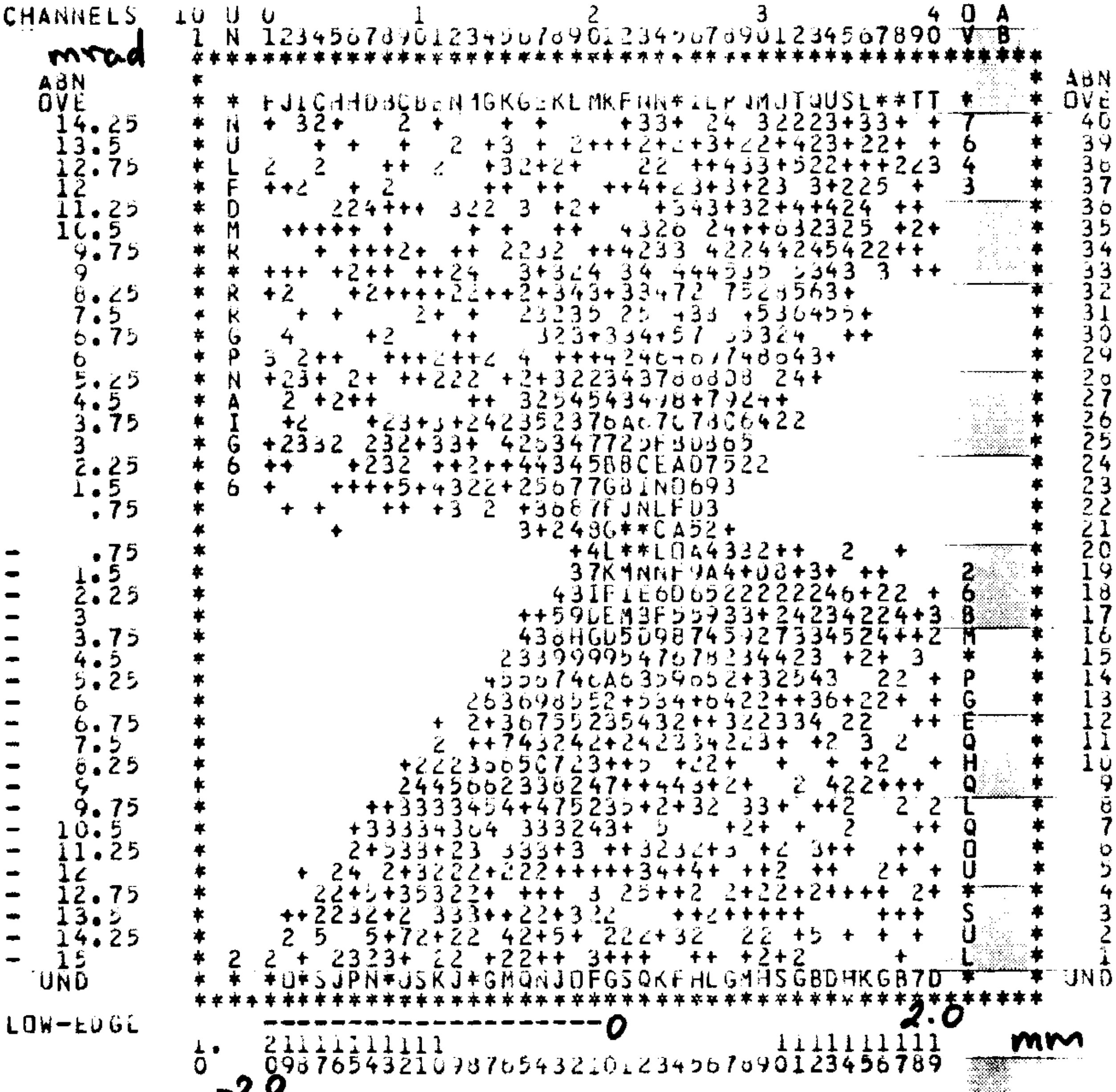


Fig. 36. Positron Population of the x-x' phase space at the focal plane. All momenta are included

* ENTRIES = 45528
* SATURATION AT= 31
* SCALE .,+,2,3,.,.,., A,B,
* STEP = 1 * MINIMUM=0

PLOT STATISTICS

| | | |
|---|---|---|
| 31 | 835 | 31 |
| 358 | 3567 | 427 |
| 31 | 835 | 31 |

POSITRON Y EMITTANCE

HBOOK ID = 104 DATE 82/04/13 NO = 33

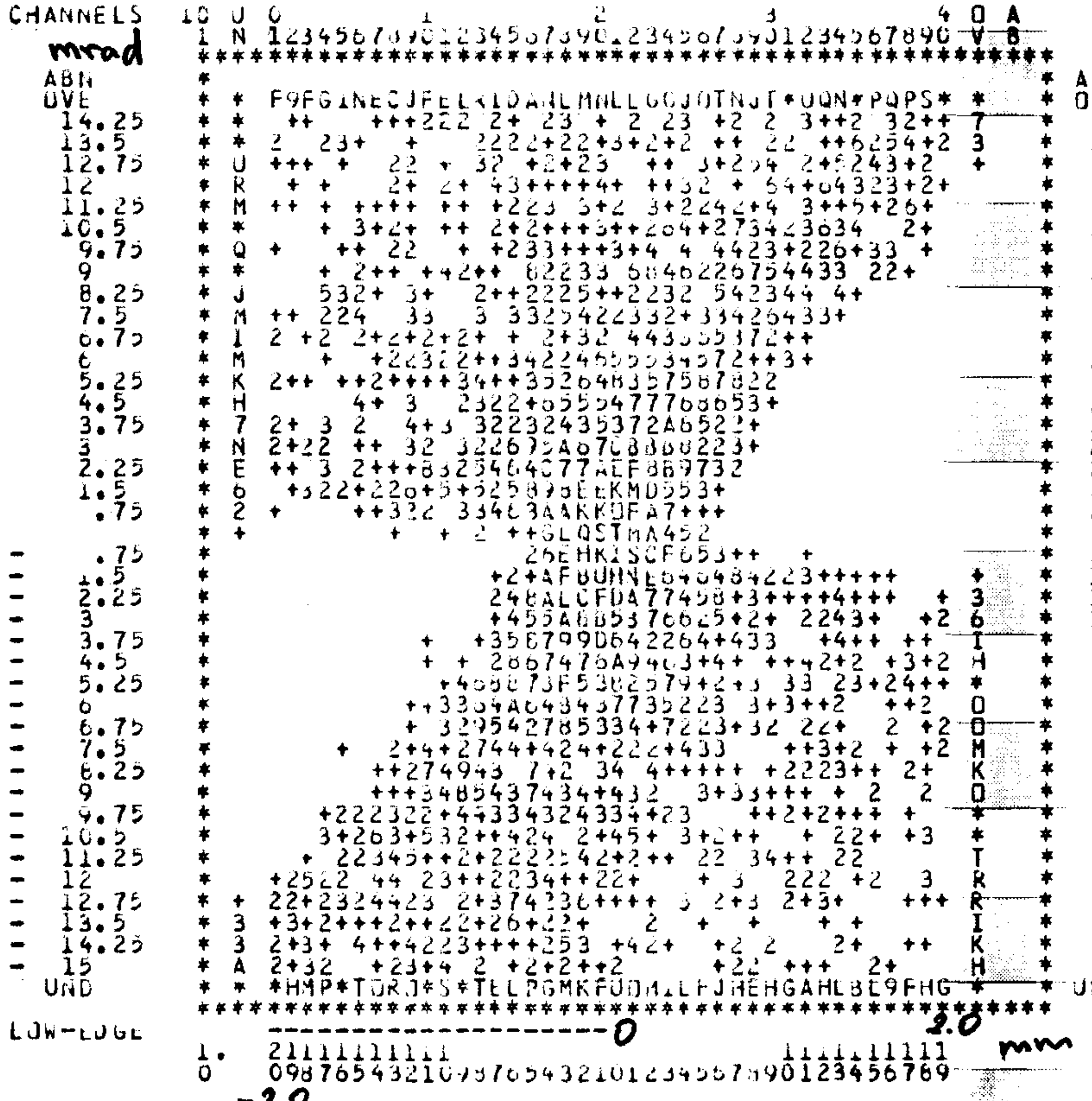


```
*
* ENTRIES =       46528                PLOT          31  I  841   I   31
* SATURATION  AT=          31                   ----------I---------I---------
* SCALE  .,+,2,3,.,.,.,  A,3,          STATISTICS    417 I 3614   I  401
* STEP =   1      * MINIMUM=0                   ----------I---------I---------
                                                     31  I  832   I   31
```

Fig. 37. Positron Population of the y-y' phase space at the focal plane. All momenta are included

ELECTRON X EM. IN MOM CUT

HBOOK ID = 106 DATE 82/04/13 NO = 35

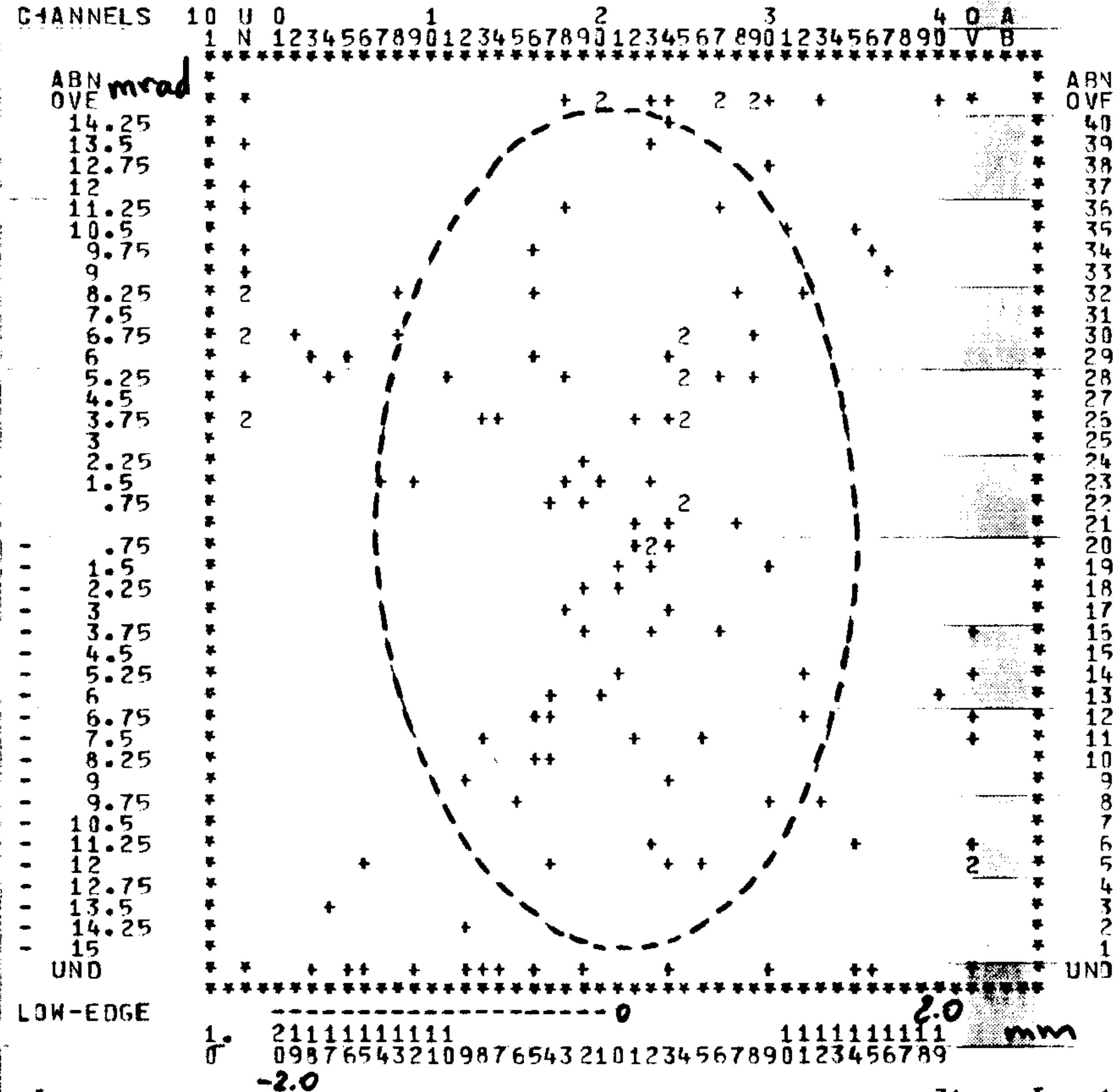


Fig. 38. No. of Electrons (72) captured within an horizontal acceptance of 20 $\pi$ mm-mrad and $\Delta E/E = \pm 5\%$ around 5 GeV

* ENTRIES = 301

* SATURATION AT= 31

* SCALE .,+,2,3,.,.,., A,B,

* STEP = 1 * MINIMUM=0

PLOT STATISTICS

| | | |
|---|---|---|
| 31 | 12 | 31 |
| 12 | 89 | 7 |
| 31 | 13 | 31 |

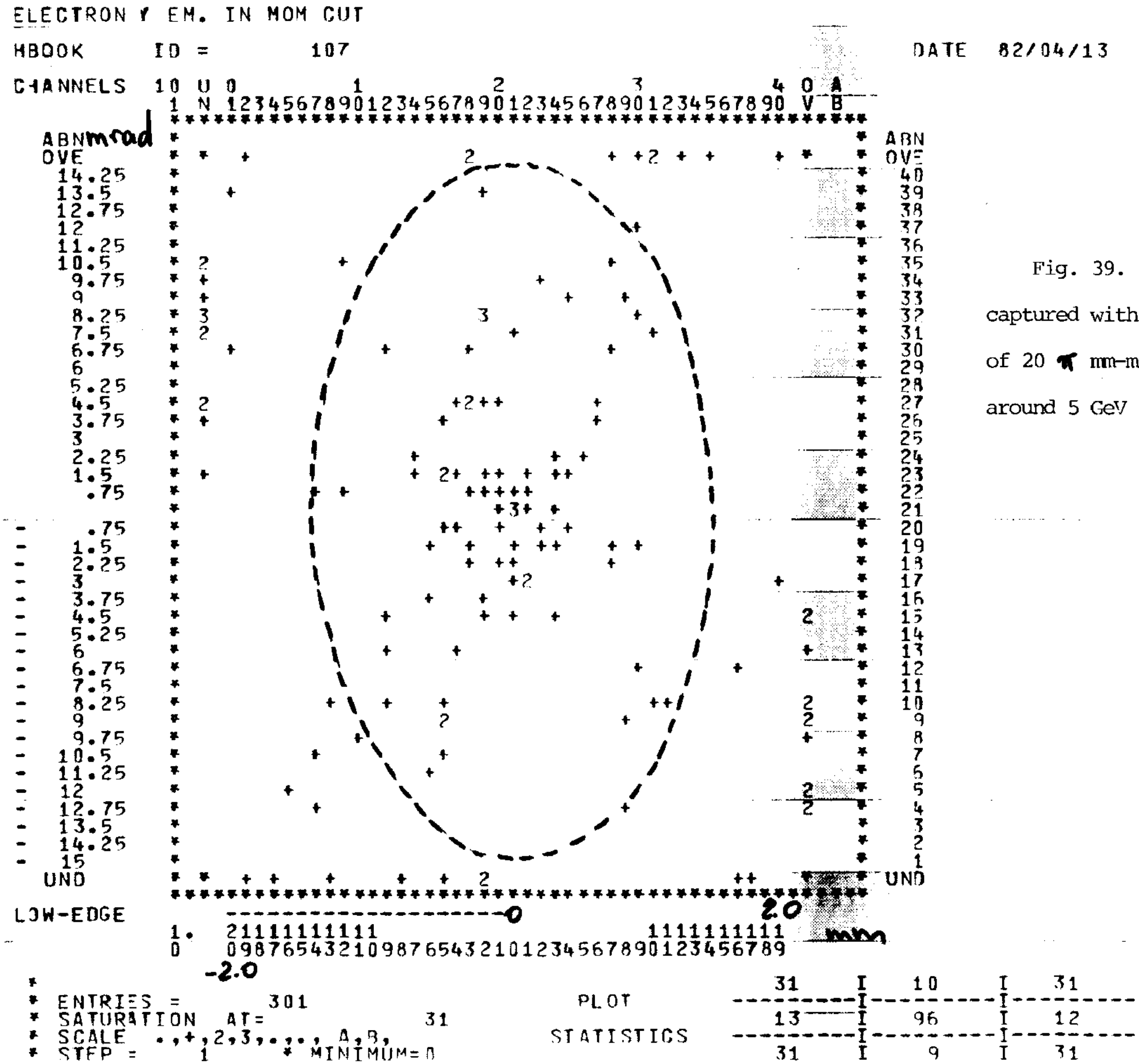


Fig. 39. No. of Electrons (84) captured within a vertical acceptance of 20 $\pi$ mm-mrad and $\Delta E/E = \pm 5\%$ around 5 GeV

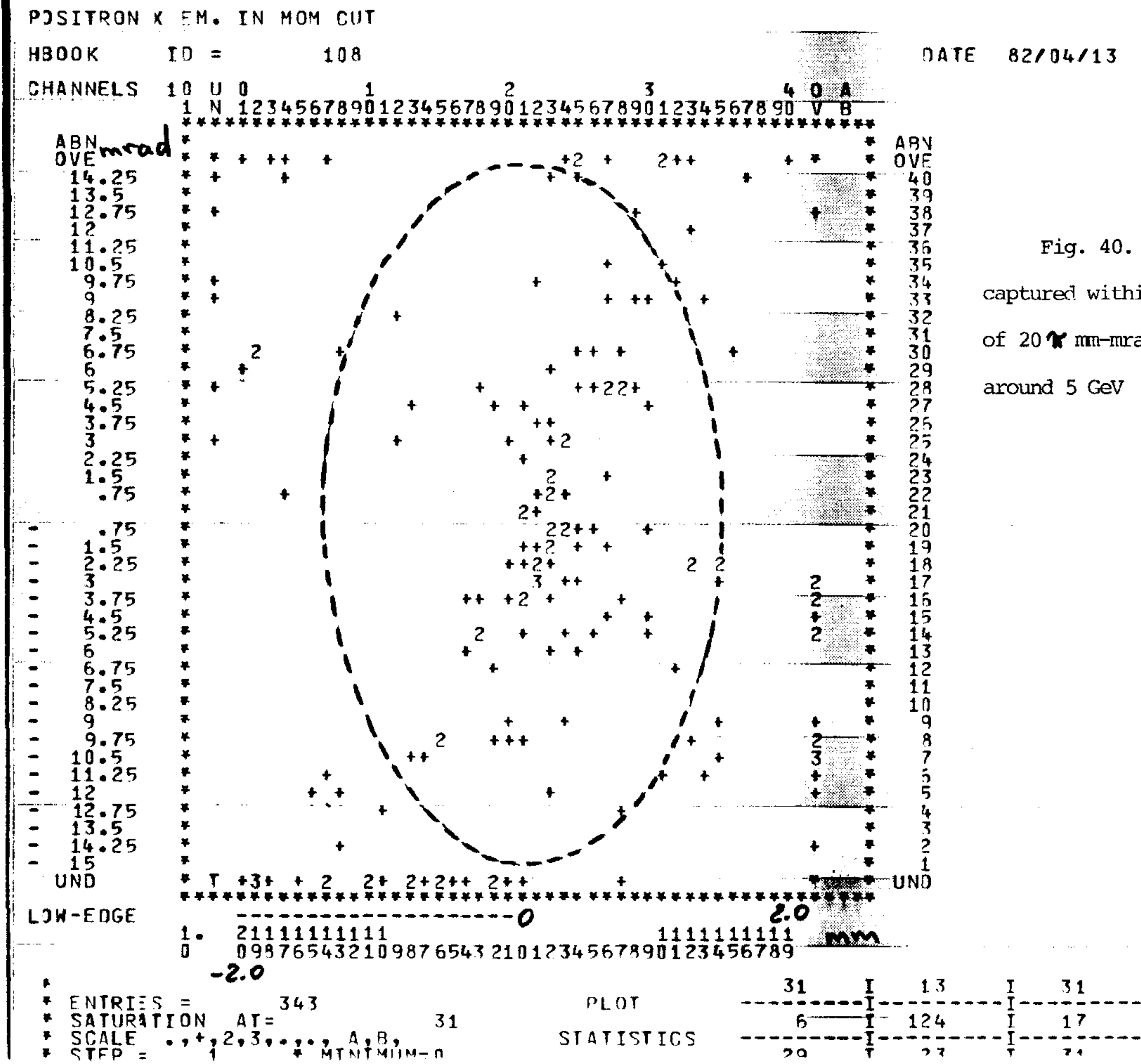


Fig. 40. No. of Positrons (100) captured within a horizontal acceptance of 20π mm-mrad and $\Delta E/E = \pm 5\%$ around 5 GeV

POSITRON Y EM. IN MOM CUT

HBOOK ID = 109 DATE 82/04/13 NO = 38

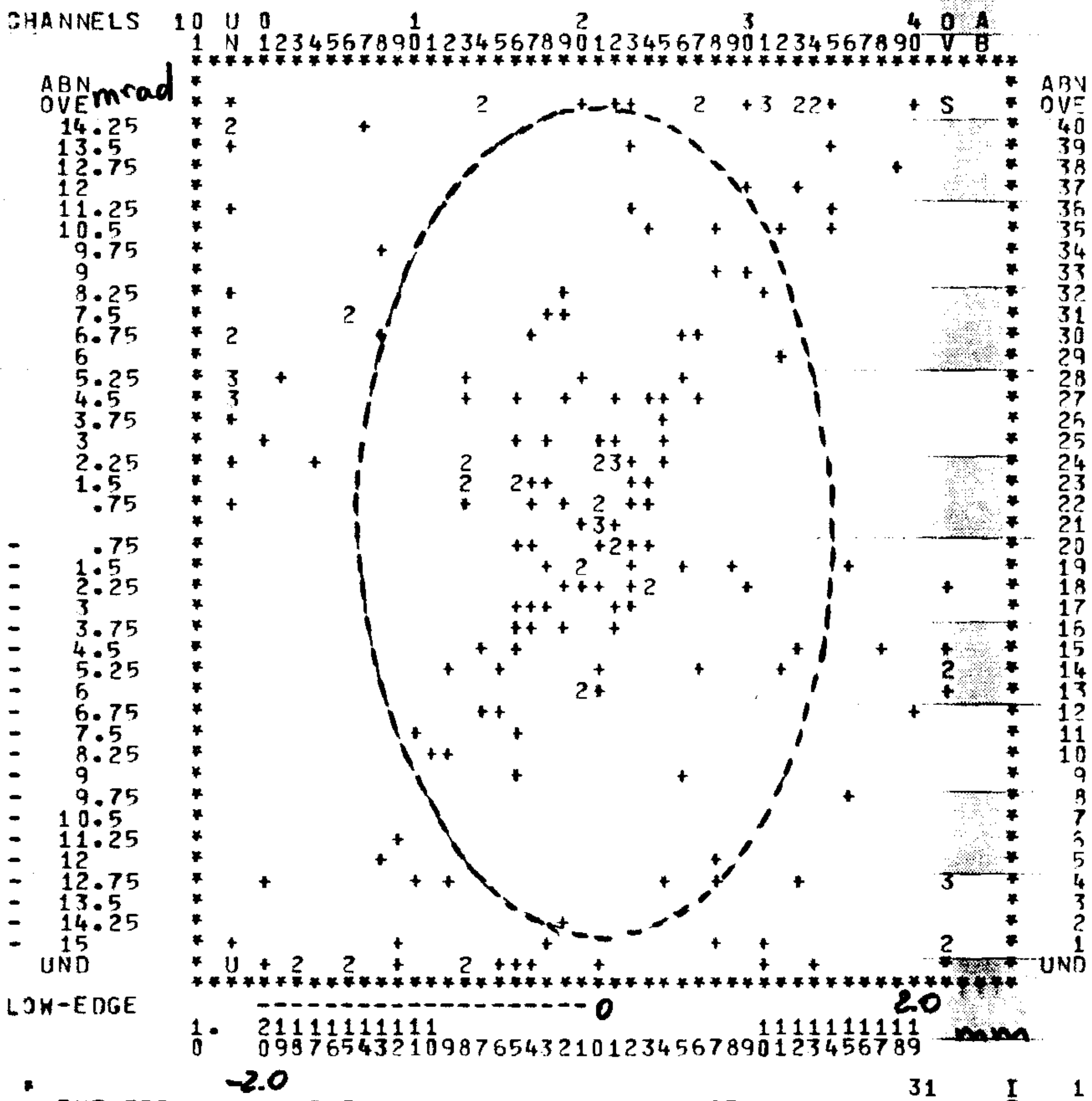


* ENTRIES = 343
* SATURATION AT= 31
* SCALE .,+,2,3,.,.,., A,B,
* STEP = 1 * MINIMUM=0

PLOT STATISTICS

| | | |
|---|---|---|
| 31 | 17 | 28 |
| 17 | 140 | 10 |
| 30 | 14 | 31 |

Fig. 41. No. of Positrons (111) captured within a vertical acceptance of 20 $\pi$ mm-mrad and $\Delta E/E = \pm 5\%$ around 5 GeV

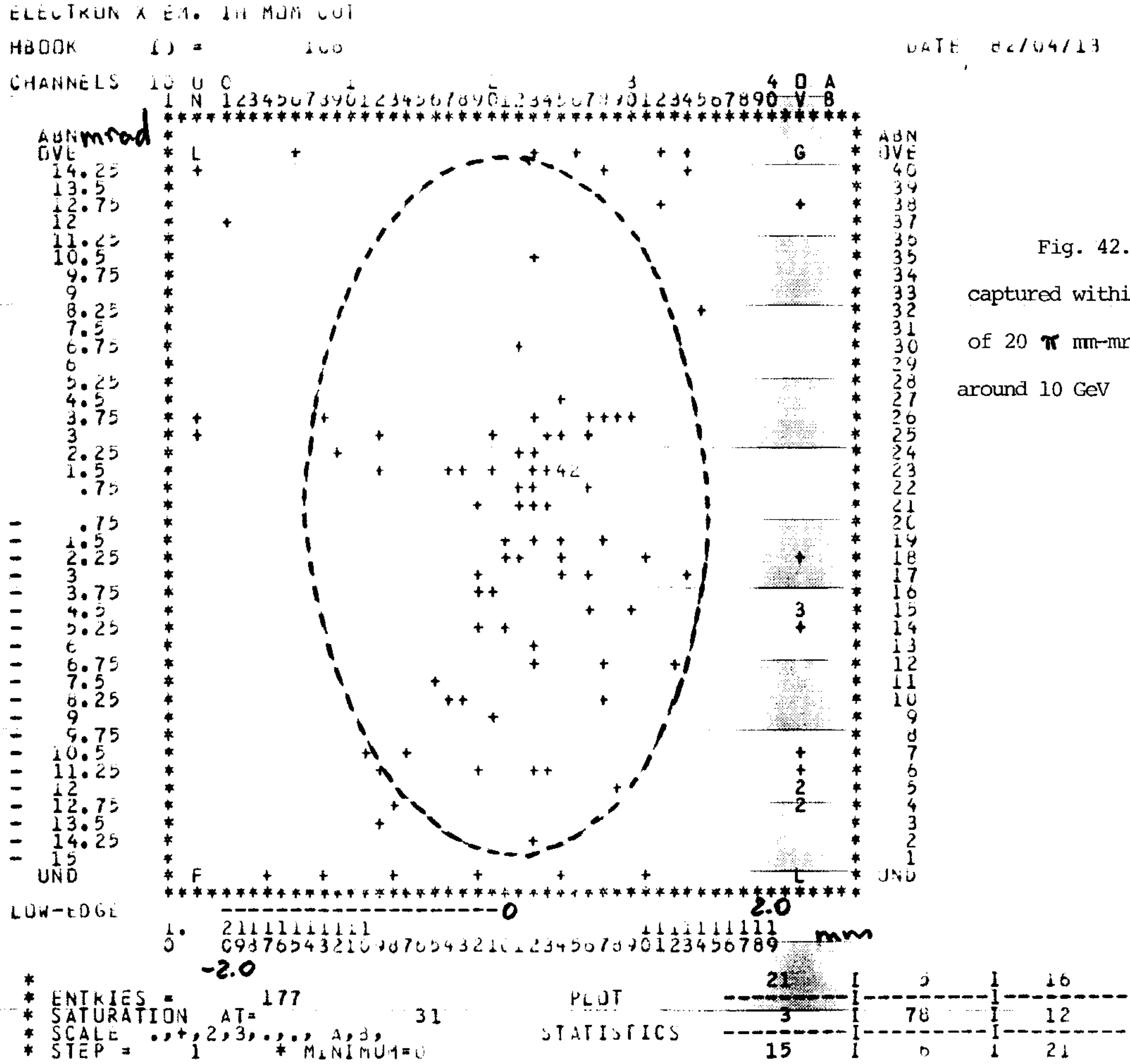


Fig. 42. No. of Electrons (69) captured within an horizontal acceptance of 20 $\pi$ mm-mrad and $\Delta E/E = \pm 5\%$ around 10 GeV

ELECTRON Y EM. IN MOM CUT

HBOOK ID = 107 DATE 82/04/13 NO = 35

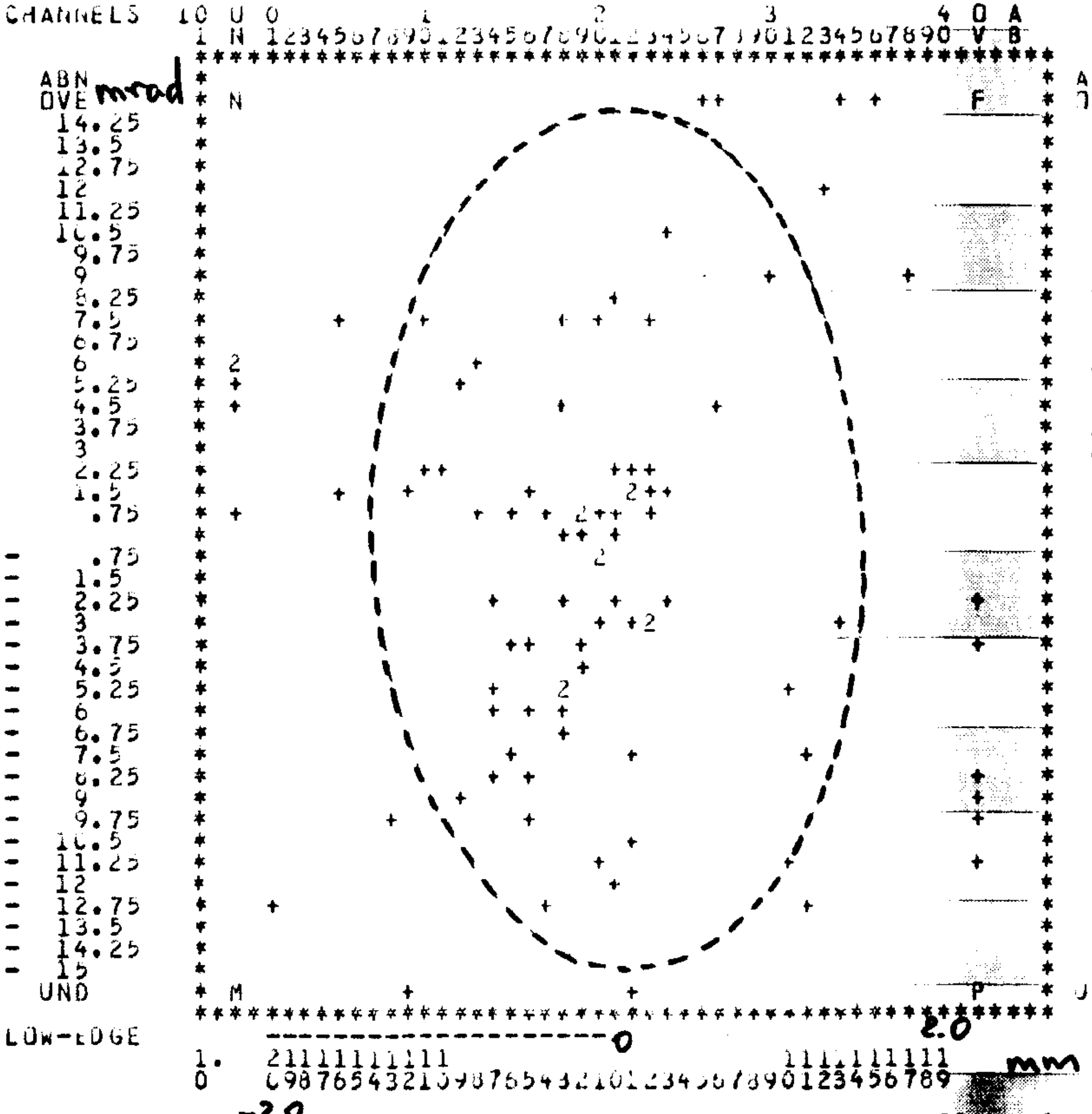


* ENTRIES = 177

* SATURATION AT= 31

* SCALE .,+,2,3,.,.,., A,B,

* STEP = 1 * MINIMUM=0

PLOT STATISTICS

| | | |
|---|---|---|
| 23 | 4 | 15 |
| 5 | 75 | 6 |
| 22 | 2 | 25 |

Fig.43. No. of Electrons (68) captured within a vertical acceptance of 20 $\pi$ mm-mrad and $\Delta E/E = \pm 5\%$ around 10 GeV

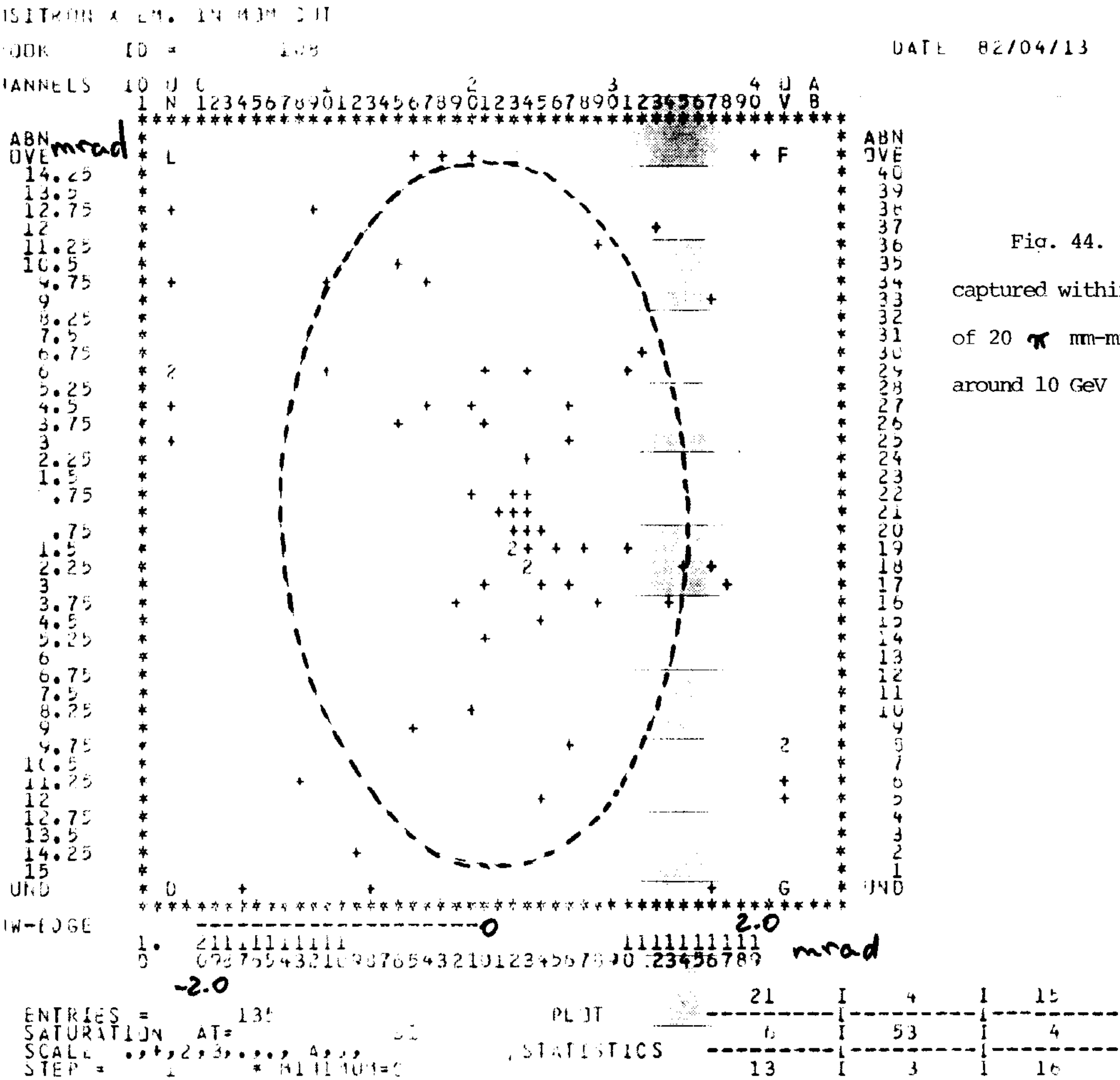


Fig. 44. No. of Positrons (45) captured within an horizontal acceptance of 20 $\pi$ mm-mrad and $\Delta E/E = \pm 5\%$ around 10 GeV

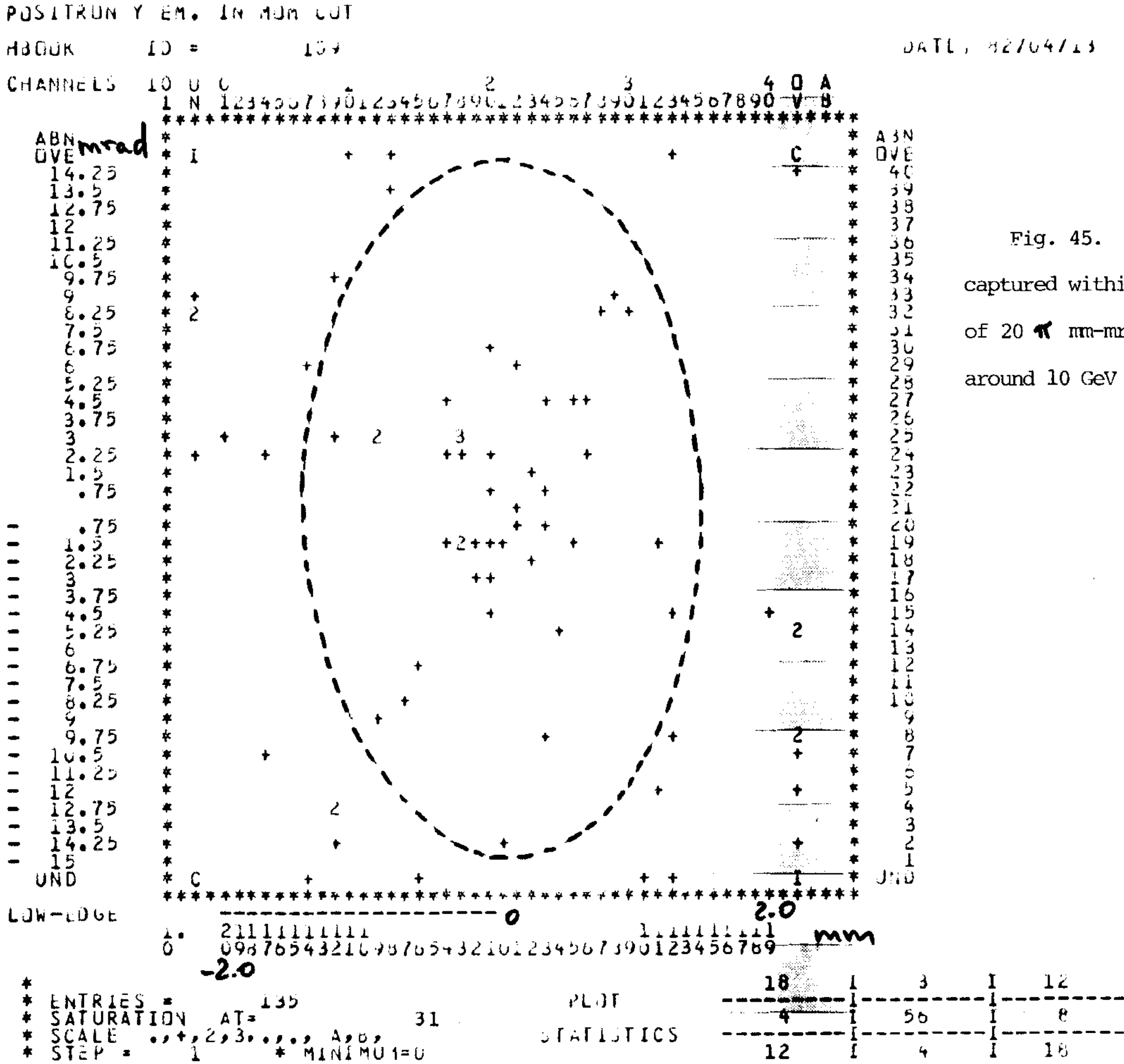


Fig. 45. No. of Positrons (44) captured within a vertical acceptance of 20 $\pi$ mm-mrad and $\Delta E/E = \pm 5\%$ around 10 GeV